AFRL-RV-HA-TR-2007-1113

Excitation of the Magnetospheric Cavity

Timothy F. Bell
Prajwal Kulkarni

STAR Laboratory
Stanford University
Stanford, CA 94305

Final Report

16 June 2007

APPROVED FOR PUBLIC RELEASE; DISTRIBUTION UNLIMITED.

AIR FORCE RESEARCH LABORATORY
Space Vehicles Directorate
29 Randolph Road
AIR FORCE MATERIEL COMMAND
Hanscom AFB, MA 01731-3010

NOTICE AND SIGNATURE PAGE

Using Government drawings, specifications, or other data included in this document for any purpose other than Government procurement does not in any way obligate the U.S. Government. The fact that the Government formulated or supplied the drawings, specifications, or other data does not license the holder or any other person or corporation; or convey any rights or permission to manufacture, use, or sell any patented invention that may relate to them.

This report was cleared for public release and is available to the general public, including foreign nationals. Qualified requestors may obtain additional copies from the Defense Technical Information Center (DTIC) (http://www.dtic.mil). All others should apply to the National Technical Information Service.

AFRL-RV-HA-TR-2007-1113 HAS BEEN REVIEWED AND IS APPROVED FOR PUBLICATION IN ACCORDANCE WITH ASSIGNED DISTRIBUTION STATEMENT.

//Signature//	//Signature//
DANIEL L. ELSNER, 2dLt Contract Manager	JOEL MOZER, Chief Space Weather Center of Excellence

This report is published in the interest of scientific and technical information exchange, and its publication does not constitute the Government's approval or disapproval of its ideas or findings.

REPORT DOCUMENTATION PAGE

Form Approved
OMB No. 0704-0188

1. REPORT DATE *(DD-MM-YYYY)*	2. REPORT TYPE	3. DATES COVERED *(From - To)*
16-06-07	Final Report	31 Oct 04 – 23 Jul 07

4. TITLE AND SUBTITLE
Excitation of the Magnetospheric Cavity

5a. CONTRACT NUMBER
F19628-03-C-0059

5b. GRANT NUMBER

5c. PROGRAM ELEMENT NUMBER
62601F

6. AUTHOR(S)
Timothy F. Bell and Prajwal Kulkarni

5d. PROJECT NUMBER
1010

5e. TASK NUMBER
RR

5f. WORK UNIT NUMBER
A1

7. PERFORMING ORGANIZATION NAME(S) AND ADDRESS(ES)

STAR Laboratory
Stanford University
Stanford, CA 94305

8. PERFORMING ORGANIZATION REPORT NUMBER

9. SPONSORING / MONITORING AGENCY NAME(S) AND ADDRESS(ES)
Air Force Research Laboratory
29 Randolph Road
Hanscom AFB, MA 01731-3010

10. SPONSOR/MONITOR'S ACRONYM(S)
AFRL/RVBXR

11. SPONSOR/MONITOR'S REPORT NUMBER(S)
AFRL-RV-HA-TR-2007-1113

12. DISTRIBUTION / AVAILABILITY STATEMENT
Approved for public release; distribution unlimited.

13. SUPPLEMENTARY NOTES

14. ABSTRACT

Stanford University carried out a detailed study of the following topics: 1) the optimum orbit for exciting the magnetospheric cavity resonance by a space-based ELF/VLF transmitter, 2) the antenna type and configuration necessary to excite various cavity modes with the radiated ELF/VLF waves, 3) the effects of Landau damping on the ELF/VLFL waves within the cavity, 4) the effectiveness of the radiated ELF/VLF cavity waves in precipitating energetic radiation belt particles, and 5) the optimum spacecraft orbit, antenna configuration, and ELF/VLF transmitter frequency spectrum for precipitating energetic radiation belt particles over a wide range of energies. In addition, a study was carried out concerning the excitation of the magnetospheric cavity by ground-based VLF transmitters.

15. SUBJECT TERMS
Space-based ELF/VLFl transmitters, Magnetospheric cavity, ELF/VLF wave propagation

16. SECURITY CLASSIFICATION OF:			17. LIMITATION OF ABSTRACT	18. NUMBER OF PAGES	19a. NAME OF RESPONSIBLE PERSON
a. REPORT	b. ABSTRACT	c. THIS PAGE			Daniel L. Elsner, 2dLt
U	U	U	UU	44	19b. TELEPHONE NUMBER *(include area code)*

TABLE OF CONTENTS

FIGURES

1. (a) Ray paths of a 5.6-kHz signal injected at $L = 1.5$ at the equator and a 2.0-kHz signal injected at $L = 2.5$ and $\lambda = 20^o$. (b) Variations of the wave power density along the ray paths at different L-shells.

2. (a) Ray path of a 2.5-kHz signal injected at the geomagnetic equator at $L = 2$ with an initial wave normal angle of -85^o. (b) An expanded portion from the ray path shown in (a). (c) The cavity enhancement factor after signal injection plus the first two equatorial crossings.

3. (a) Ray path of a 2.5-kHz ($\sim$ local f_{LHR}) signal injected at the equator at $L =$ 2 at a wave normal angle of -75^o. (b) Normalized wave power along the ray path. (c) Cavity enhancement factor at equator as a function of L-shell. (d) Ray path for a wave injected at a wave normal angle of -85^o. (e) Wave energy persists for a longer time when the injection wave normal increases. (f) Cavity enhancement also increases when the injection wave normal angle increases. (g) An almost perpendicular injection wave normal angle almost results in numerous magnetospheric reflections near the $L = 2$ shell. (h) This signal persists for many tens of seconds. (i) The cavity enhancement factor is even larger with an injection wave normal angle of -89^o.

4. (a) - (f) Similar to before, but for 1-kHz and 4 –Hz waves.

5. Cavity enhancement factor integrated over all wave normal angles considered. Result is normalized by the total number of injections. The cavity enhancement is shown at L-shells from $1 < L < 3.5$ for 1-kHz, 2.5-kHz and 4-kHz waves injected from $L = 2$; with equatorial injections shown across the top row and off-equatorial across the bottom row.

6. The three columns display the three sample wave frequencies of 1 kHz, 2.5 kHz, and 4 kHz; and each row represents the three separate injection source sites ($L = 1.5$, 2.0 and 2.5). All waves were injected from the magnetic equator.

7. Integrated cavity enhancement factor for injection from the geomagnetic equator at L = 1.5 , where the equatorial f_{LHR} is approximately 6 kHz.

8. (a) – (i) Similar to before, with parameters indicated on plots. All rays were injected at $L = 2$ at $\lambda = 20^{o}$.

9. The effects of incorporating the frequency and angular limitations imposed by the use of short antennas in a magnetoplasma

10. (a) - (c) $Y = | \psi - \psi_{res} |$ for three different wave frequencies and initial wave normal angles, all injected from the equator at $L = 2$. The quasi-periodicity seen is a result of repeated magnetospheric reflections along the raypath. Note that regardless of frequency or initial wave normal angle, ψ rapidly ends up very close to the resonance cone.

11. Differential number flux at 100 km altitude induced by an equatorial source at $L = 2$. The left (right) two columns display the flux induced at the northern (southern) hemisphere.

12. The top panel shows resonant electron energy along the raypath for the m = 1 resonance mode for a 3.5-kHz wave injected from the equator at $L = 2$. The bottom panel shows geomagnetic latitude along raypath. Note that E_{res} increases off the equator, and that the resonant energy stays above 100 keV at all points along the raypath.

13. Differential number flux in the northern hemisphere at $L = 2$ and $L = 1.9$ induced by a 3.5 kHz equatorial source at $L = 2$. These results used a constant energetic electron distribution function of 50,000 cm^{-2}-s^{-1}-$ster^{-1}$-keV^{-1} with a square loss-cone.

14. Precipitation and illumination spectra induced by sources at $L = 2$, at the geomagnetic equator and a latitude of 20^{o} . These results were obtained by integrating the differential number flux over time.

15. Similar to Figure 14, except for sources at L = 2.5 . Although the region of illumination is at higher L-shells, the general trends are similar and explained in the text.

16. Raypaths, Landau damping and latitude along raypath for two 3.5-kHz rays injected from L = 2. The left column displays these parameters for a ray with an initial wave normal angle of -88^{o}, while the right column is for $\psi = 0^{o}$.

17. Precipitation spectra for 3.5-kHz waves injected at a range of initial wave normal angles. Note that lower initial ψ spreads wave power over a broader range of L-shells, but the precipitation signature is generally weaker at higher energies.

1. SUMMARY

During the period of performance, Stanford University carried out a detailed study of the following topics: 1) the optimum orbit for exciting the magnetospheric cavity resonance by a space-based extremely low frequency/very low frequency (ELF/VLF) transmitter, 2) the antenna type and configuration necessary to excite various cavity modes with the radiated ELF/VLF waves, 3) the effects of Landau damping on the ELF/VLF waves within the cavity and possible methods of minimizing this damping, 4) the effectiveness of the radiated ELF/VLF cavity waves in precipitating energetic radiation belt particles, and 5) the optimum spacecraft orbit, antenna configuration, and ELF/VLF transmitter frequency spectrum for precipitating energetic radiation belt particles over a wide range of energies.

2. INTRODUCTION

Enhanced fluxes of energetic radiation belt electrons represent a dangerous threat to United States civilian and military space assets. This enhancement could result, for example, from a series of large coronal mass ejections from the sun. Orders-of-magnitude increase in the radiation belt energetic electron fluxes can reduce the lifetime of important space assets by orders-of-magnitude.

One possible method of reducing enhanced fluxes of radiation belt electrons is to introduce ELF/VLF waves into the belts. Resonance interactions between very low frequency, or whistler-mode, waves and energetic electrons are believed to play a significant role in the loss of trapped particles in the near-earth space environment [*Kennel and Petschek*, 1966; *Lyons et al.*, 1972; *Abel and Thorne*, 1998a]. Such waves occur naturally, for example, in the form of plasmaspheric hiss, VLF chorus and lightning-generated whistlers. Powerful ground-based VLF transmitters also inject VLF waves into the radiation belts. These transmitters operate continuously and radiate signals that illuminate the Earth-ionosphere waveguide for naval communication. However, a portion of this wave energy inevitably leaks into the magnetosphere where the injected waves interact with and precipitate radiation belt electrons.

The main objective of this contract is to determine the effects of waves from space-based ELF/VLF transmitters upon energetic electrons in the radiation belts. These waves are trapped in the magnetospheric cavity and reflect internally many times before they are absorbed by Landau damping. While they are trapped in the cavity, these waves can continuously scatter energetic electrons from the radiation belts. Our study concerns the following topics: 1) the optimum orbit for exciting the cavity resonance by a space-based ELF/VLF transmitter, 2) the antenna type and configuration necessary to excite various cavity modes with the radiated ELF/VLF waves, 3) the effects of Landau damping on the ELF/VLF waves within the cavity and possible methods of minimizing this damping, 4) the effectiveness of the radiated ELF/VLF cavity waves in precipitating energetic radiation belt particles, and 5) the optimum spacecraft orbit, antenna configuration, and ELF/VLF transmitter frequency spectrum for precipitating energetic radiation belt particles over a wide range of energies.

3. RESULTS

We address the major portions of our study concerning the five items listed in the Summary. Specifically, we report simulation results which indicate that only three space-based sources are needed to completely fill the plasmasphere with ELF/VLF wave energy. These simulations incorporated the *Wang and Bell* [1970] model that describes the radiation of an electric dipole immersed in a magnetopolasma, as well as the effects of Landau damping in the plasmaspheric cavity. These results have been published in the peer-reviewed literature [*Kulkarni et al*., 2006].

3.1. Illumination of Plasmaspheric Cavity

Numerical ray tracing indicates that the in-situ injection of whistler-mode waves of 1 kHz to 4 kHz can be used to illuminate the inner radiation belts and slot region. These results were derived by using the Stanford VLF Ray Tracing Program to simulate sources placed at a total of six points in the inner magnetosphere: $L = 1.5$, $L = 2.0$ and $L=2.5$ at two geomagnetic latitudes, the equator and a latitude of 20^o along each field-line. The results demonstrate that an in-situ source, by varying the frequency of the injected waves, can illuminate L-shells both higher and lower than the source site, with wave frequencies below (above) the local lower hybrid resonance, f_{LHR} moving to higher (lower) L-shells. We restrict the radiating wave frequency, f, to $0.9\, f_{LHR} < f < (f_{LHR} + 1$ kHz), and the wave normal angle at injection to no farther than 3^o from the resonance cone. Even after accounting for these restrictions, it appears to require only three in-situ sources placed at the above locations to illuminate $1.4 < L < 2.7$, which comprises the bulk of the inner radiation belt.

We utilized the Stanford VLF ray tracing code [*Inan and Bell*, 1977] coupled with an accurate estimation of the path-integrated Landau damping to determine the distribution of wave energy throughout the inner radiation belts based on injection location, wave frequency, and injection wave normal angle. The Stanford VLF ray tracing code models the geomagnetic field as a centered dipole with an electron gyrofrequency of 880 kHz at the ground at the equator, and uses a diffusive equilibrium model [*Angerami and Thomas*, 1964] to calculate charged particle densities. Adopting a different density profile (such as given by *Carpenter and Anderson* [1992]) does not significantly change the region of illumination ($\pm 0.2L$) or cavity enhancement factors (± 0.5) for the frequencies considered (see below). For this study, we considered a cold, smoothly varying plasma without any ducts or density irregularities.

We primarily focus on a single transmitter near the magnetic equatorial plane at $L = 2$ and consider both equatorial and off-equatorial injection points for wave frequencies ranging from well below, to well above, the local lower hybrid resonance (LHR) frequency and also for a broad range of injection wave normal angles. We initially neglect the effects of antenna radiation in a magnetoplasma in order to facilitate a more complete picture of whistler-mode wave propagation in the inner magnetosphere as a result of in-situ injection. We, then, modify these results by incorporating the limitations

that would be imposed by the radiation pattern [*Wang and Bell,* 1970] for a short electric dipole radiating in a magnetoplasma.

3.1.1. Magnetospheric Cavity Enhancement Factor

As noted by *Edgar* [1976], whistler-mode waves in the magnetosphere can undergo total internal reflections as they propagate from regions where the wave frequency is above the lower hybrid frequency to points where $f \sim f_{LHR}$. This reflection process can occur numerous times with the magnetosphere, thus, constituting a resonant ELF/VLF cavity wherein repeated reflections may lead to enhancement of wave energy. To properly quantify the manner in which wave energy is distributed within the magnetosphere, we must properly account for the fact that successive reflections may cause wave energy represented by a single injected ray to cross the same region numerous times before the wave power is significantly damped. To this end, we introduce the concept of the magnetospheric cavity enhancement factor (see below) to quantify the combined effects of magnetospheric reflections and Landau damping along the ray path.

Landau damping, the primary damping mechanism for obliquely propagating whistler waves in the collisionless magnetospheric medium, is calculated using the formulation of *Brinca* [1981] and an electron distribution of $f(v) = 2 \times 10^5 v^{-4}$ cm^{-6}-s^3 as an approximate fit to recent energetic electron measurements [*Bell et al.*, 2002]. Figures 1a and 1b show two sample ray paths, as calculated using the Stanford VLF ray tracing code [*Inan and Bell*, 1977], and the associated Landau damping for each path. The ray path and attenuation change dramatically with the input parameters, as is examined in greater detail below.

Spacecraft observations indicate that a single whistler-mode wave can magnetospherically reflect up to at least 40 times before being significantly damped [*Smith and Angerami*, 1968; *Edgar*, 1976; *Gurnett and Inan*, 1988], resonantly interacting with, and pitch angle scattering, energetic electrons at all points along the ray path. We, nevertheless, focus our attention on the magnetic equator because the slow variation of the Earth's magnetic field at that point allows for the longest interaction time for wave-particle interactions and, hence, the highest diffusion (or scattering) coefficients. We, then, divide the magnetic equator into equally sized radial ``bins" of 0.1L in length, for example, and, for each equatorial crossing, note the location of the ray in L-shell and assign it to the appropriate L-bin. To arrive at the cavity enhancement factor for each L-bin, we simply sum the normalized wave power (i.e., starting with a value of unity at the injection point) for every crossing of that bin by any ray.

To illustrate this concept more clearly, consider the ray path, shown in Figure 2a, of a 2.5-kHz wave injected from $L = 2$ at the magnetic equator with an initial wave normal angle of -85^o. For simplicity, only the injection and the first two equatorial crossings are expanded (shown in more detail in Figure 2b), along with the normalized wave power as attenuated by Landau damping and the location in the L-shell of the ray at each magnetic equatorial crossing. Next, we divide the magnetic equator into bins such

that the ray position at injection (L = 2.0) and first equatorial crossing (L = 2.08) are both assigned to the L = 2.0 shell, and the ray position at the second equatorial crossing (L = 2.13) is assigned to the L = 2.1 shell. Finally, for each L-bin, we sum the normalized wave power of the ray at every equatorial crossing within that bin to determine the resulting cavity enhancement factor.

Referring again to Figure 2b, the cavity enhancement at the L = 2.0 shell is 1.996 (normalized power of 1.0 at injection plus a ray power of 0.996 at the first crossing) and 0.992 at the L = 2.1 shell. Of course, had we examined more than just the first two crossings, the cavity enhancement factor at both the L = 2.0 and the L = 2.1 regions may have been higher and the ray may also have propagated (and, thus, carried wave energy) to additional L-shells. Figure 2c displays the cavity enhancement factor at the L = 2.0 and L = 2.1 shells after the first two equatorial crossings. It is important to note that a cavity enhancement factor greater than unity does not imply amplification of the wave power; it simply represents the fact that, for example, an injected signal of 1-sec duration would cross the geomagnetic equator multiple times over a time period longer than 1-sec, scattering electrons each time. A cavity enhancement factor of 1.5 would imply that this signal could be 1.5 times more effective in pitch-angle scattering than it would have been in the absence of magnetospheric reflections. Alternatively, for the case of injection of a continuous wave train, we can think of the enhancement factor as the factor by which the total wave power multiplicatively increases with time as the wave energy is stored within the cavity. The magnetospheric reflections allow a single wave packet to interact with the energetic particles multiple times, with the wave power density decreasing with time. Accordingly, with several equatorial passes, the cumulative normalized power at a given L-shell region is greater than unity.

3.1.2. Simulation Results

Our objective, as discussed above, is to quantify the projection of electromagnetic wave power onto a specific L-shell region from a particular injection point in space. At any given time, it may be desirable to project wave power either to regions close to the satellite location or to L-shells far away from the source. The input parameters (wave frequency and wave normal angle at injection) are likely to be different depending on the location of the satellite and the region where we wish to project wave power. We, therefore, simulate a substantial number of rays with a range of input parameters so that conclusions can be drawn with regards to appropriate frequencies and wave normal angles. One particular question of practical interest is how to determine the number and location of in-situ sources needed to completely illuminate the region $1.3 < L < 3.5$ with ELF/VLF whistler-mode wave energy.

The simulation procedure we use is as follows: We, first, start with a given injection L-shell and magnetic latitude. We consider three such L-shell locations -- L = 1.5, L = 2.0 and L = 2.5 -- as well as two geomagnetic latitudes, the equator and a latitude of 20^o along each field line. This set of parameters constitutes a total of six different injection source sites. For each source site, we then inject waves at 100 different frequencies ranging from 1-10 kHz, in increments of 0.1 kHz, and, for each wave

frequency, with initial wave normal angles from -75^o up to the resonance cone if $f > f_{LHR}$ or up to -89.9^o for $f < f_{LHR}$, with each wave normal angle separated by 0.1^o. For each ray, we also calculate the path-integrated Landau damping and the cavity enhancement factor at the geomagnetic equator. The frequency range is chosen to encompass frequencies ranging from well below the local LHR frequency at all equatorial regions in the inner radiation belts up to a frequency for which magnetospheric reflections no longer occur.

The bulk of the simulation results shown are for a source located at $L = 2$ for which we separately examine equatorial and off-equatorial injections. However, before presenting the bulk of the simulation results, it is instructive to briefly explore whistler-mode wave behavior in the inhomogeneous magnetospheric medium, especially the phenomena of the wave energy settling on a prescribed *L*-shell (dependent only on wave frequency) and also the relationship between initial wave parameters (frequency, wave normal angle) and the lifetime (i.e., cavity enhancement factors).

3.1.3. *L*-Shell Settling and Wave Lifetimes

Whistler-mode waves propagating in the magnetosphere have the strong tendency, within the course of few initial magnetospheric reflections, to settle on an *L*-shell where the wave frequency is approximately equal to the equatorial f_{LHR} [*Thorne and Horne*, 1994 and *Ristic'-Djurovic' et al*., 1998]. Manipulation of the wave frequency thus represents a first-order means for controlling the illumination of a particular *L*-shell. The LHR frequency [$f_{LHR} \sim (f_{He} f_{Hi})^{1/2}$ for $L = 2$, where f_{He} is the electron gyrofrequency and f_{Hi} is the ion gyrofrequency] is generally larger at locations closer to the Earth's surface. To selectively target lower *L*-shell field lines, frequencies higher than the local LHR should be used, while lower frequencies should be used to project power toward higher *L*-shells. This behavior is a strong function of wave frequency and does not change substantially with the injection location (*L*-shell and geomagnetic latitude) or injection wave normal angle, although some exceptions will be noted. However, waves with an initially smaller normal angle or waves injected off the magnetic equator tend to propagate farther from their injection point before returning back, thereby taking a longer time to reach their settling *L*-shell.

The presence of path-integrated Landau damping greatly limits the ability of a whistler-mode wave of a given frequency to reach its settling *L*-shell without significant power loss. For in-situ injections, waves injected above the local f_{LHR} or off the geomagnetic equator experience especially strong damping [*Bortnik et al*., 2003a].

3.1.4. Injections at the Geomagnetic Equator

We, first, consider a single-wave injection source at $L = 2$ at the magnetic equator radiating 2.5-kHz waves, just below the local lower hybrid resonance frequency (~2.55 kHz). Such waves tend to propagate slightly outward and are damped more slowly than waves with frequencies higher than the local f_{LHR} [*Bortnik et al.*, 2003a]. The resultant ray path and damping are also dependent on the wave normal angle at injection, with wave normal angles initially closer to the resonance cone persisting much longer and

resulting in larger cavity enhancement factors. This point is illustrated in Figure 3, which shows that, for 2.5-kHz waves, changing the wave normal at injection (ψ) from -75^o to -85^o to -89^o results in progressively longer ray lifetimes and larger cavity enhancement factors. However, the rays injected with $\psi = -75^o$ and -85^o disperse much farther than the ray injected $\psi = -89^o$ and, hence, can interact with energetic electrons over a broader range of L-shells. Examining rays injected at a continuum of normal angles from -75^o to -89.9^o indicates that, although 2.5-kHz waves usually propagate slightly outward from $L = 2$, certain L-shells can be preferentially targeted by carefully choosing the injection wave normal angle.

For comparison purposes, we also show the effect of injecting, from $L = 2$ at the geomagnetic equator, waves with frequencies both well below and above the local f_{LHR} of 2.55 kHz. As stated earlier, waves at a frequency below (above) the local f_{LHR} generally move to higher (lower) L-shells and are also damped more slowly (quickly). As a consequence of longer lifetimes, lower frequency waves also tend to attain overall larger cavity enhancement factors, although the L-shell regions of wave energy deposition differs from that of higher frequency waves. Figure 4 demonstrates these effects by showing the result of injection, again from $L = 2$ at the equator, of both a 1-kHz wave with $\psi = -85^o$ and a 4- kHz wave with $\psi = -85^o$. The 1-kHz wave immediately propagates to higher L-shells and persists for well over 60 seconds, whereas the 4- kHz wave moves closer to the Earth and its normalized power is reduced by ~10 dB within 10 seconds. Additionally, the maximum equatorial cavity enhancement factor for the 1-kHz ray occurs at $L \sim 2.8$, but occurs at $L \sim 2.0$ for the 4- kHz ray. Although the ray path in Figure 4 for the 4- kHz wave migrates down to $L \sim 1.7$, strong Landau damping prevents significant wave power from reaching those lower L-shells.

Our results indicate that it may be particularly difficult to project wave power to some regions of the magnetosphere with a single source located at $L = 2$. Attempting to direct wave energy to $L = 1.3$, for example, would require the use of higher frequency (~9-kHz) waves that often tend not to undergo magnetospheric reflections and that also would be Landau damped very quickly. Alternately, taking advantage of cavity enhancement at L-shells as far away as $L = 3.5$ is not possible with a single equatorial source at $L = 2$ even when 1-kHz waves are used (see top row of Figure 5). To fill larger regions of the plasmasphere with whistler-mode wave energy, one must, therefore, vary the radial distance where the satellite is placed. For injections from locations closer to the earth, we expect that the higher f_{LHR} imply that higher frequencies should be used to target the source L-shell while lower frequencies should be used for injection sites farther from the earth. As described previously, we examine the wave power propagation from in-situ sources located at $L = 1.5$ and $L = 2.5$ and, to compare with the results shown earlier for a satellite located at $L = 2$, for 1- kHz, 2.5-kHz and 4-kHz waves.

While at $L = 2$, these three frequencies are below, approximately equal to, and above the f_{LHR}, respectively, and at $L = 1.5$, all three frequencies are well below the local f_{LHR} (~6 kHz). Accordingly, injections from $L = 1.5$ at these wave frequencies propagate to higher L-shells and exhibit very high cavity enhancement factors as a result of longer lifetimes. This result can be seen in Figure 6, showing a comparison of the integrated

cavity enhancement factor (integrated along the ray path, then normalized, over all wave normal angles considered), for 1-kHz, 2.5-kHz, and 4-kHz waves, for injections from the equator at L = 1.5, L = 2.0, and L = 2.5. The top two rows of Figure 6 show injections from L = 1.5 and L = 2.0, with the 2.5-kHz waves injected from L = 1.5 having an integrated cavity enhancement factor at L = 2 that is a factor of ~4 higher than 2.5-kHz waves injected from L = 2. This result underscores the fact that wave frequencies below the local f_{LHR} — such as 2.5-kHz waves at L = 1.5 — persist for longer times than waves above the f_{LHR}.

Also note that, since the equatorial f_{LHR} is ~6 kHz, all three frequencies shown exhibit cavity enhancement primarily at L-shells higher than L = 1.5. On the other hand, for 5-kHz, 6-kHz, and 7-kHz waves, corresponding to just below, approximately equal to and above the local f_{LHR}, Figure 7 shows that the L = 1.5 region can be more effectively illuminated by simply changing the input wave frequency. It is interesting to observe that, even at a frequency of 7 kHz, field lines for L < 1.3 are not illuminated because of very rapid Landau damping and fewer magnetospheric reflections. Taking advantage of cavity enhancement at locations extremely close to the Earth's surface (1.1 < L < 1.3) may, therefore, require sources placed at those L-shells.

In order to explore wave propagation from L = 2.5 (equatorial f_{LHR} ~1.3 kHz), we refer to the bottom row in Figure 6, which displays the integrated cavity enhancement factor at 1 < $\underline{L}$ < 4 for 1-kHz, 2.5-kHz, and 4-kHz waves. As opposed to the previous source locations, 2.5-kHz and 4-kHz waves injected from L = 2.5 are above the local f_{LHR}; they, therefore, propagate down to lower L-shells and get damped more quickly than similar frequency waves injected from L = 1.5 and L = 2.0. Interestingly, even though 1 kHz is below the f_{LHR} at all three source sites considered, injections from L = 2.5 still cause substantially lower integrated cavity enhancement factors. Despite the smaller cavity enhancement, the results demonstrate that, for the sample frequencies shown, a single source at the geomagnetic equator at L = 2.5 can effectively illuminate at L-shells from L ~ 2.1 up to L ~ 3.2. This illumination range does not increase significantly with the inclusion of additional, higher frequencies because these frequencies would be damped before reaching their settling L-shell.

3.1.5. Off-Equatorial Injections

Up to this point, we have considered wave injection from sources located solely at the geomagnetic equator. In practice, any spacecraft-based source in orbit would necessarily spend a lot of time at locations off the equator; it is thus useful to consider the injection of waves from such a source at other locations. For the simulations considered here, insight into the differences between equatorial and off-equatorial injections can be gained by comparing the results in Figure 8 with the results shown earlier in Figure 3. Here, we inject three 2.5-kHz rays from L = 2 at a geomagnetic latitude of 20°, with initial wave normal angles of -75°, -85° and -89°, respectively. For each case, the off-equatorial injection leads to more rapid damping of the wave and illumination of a wider range of L-shells than the corresponding equatorial injection.

Referring to Figure 6, we can see the differences more clearly between the two different source sites considered. The top row shows the integrated cavity enhancement factor for 1-kHz, 2.5-kHz, and 4-kHz waves injected from $L = 2$ at the geomagnetic equator. The off-equatorial injections, shown in the bottom row, consistently result in smaller integrated cavity enhancement factors but illuminate a broader range of L-shells. For instance, 2.5-kHz waves injected at the equator from $L = 2$ project power up to $L = 2.5$ with a normalized integrated enhancement factor as high as ~6; injections from 20^o can affect L-shells as far as $L = 2.7$ but also result in lower cavity enhancement factors. While similar results can be also be demonstrated for injections from $L = 1.5$ and $L = 2.5$, they are not shown here for the sake of brevity.

The tradeoff between greater, more localized cavity enhancement factors for equatorial injections versus smaller, more distributed cavity enhancement factors for off-equatorial injections may be important in the design of a practical system for controlled precipitation of radiation belt electrons.

3.1.6. Effects of Antenna Radiation Pattern

Our discussions, thus far, indicate that whistler-mode wave energy injected in situ from a given position can be efficiently (i.e., with relatively large cavity enhancement factors) directed to an L-shell region as far away as ~0.3L from the source for locations closer to the Earth and up to ~1L for locations farther from the earth. In formulating these results, we did not consider the restrictions that would inevitably be present as a result of the dramatically different radiation properties of practical antennas immersed in a magnetosplasma. We now investigate the effects of practical antenna efficiency and radiation pattern on our results using the model presented by *Wang and Bell* [1970] of a short electric dipole transmitting antenna immersed in a cold, magnetized plasma. In adapting the *Wang and Bell* [1970] model to our results, we note that they ignored the complicating effects of the plasma sheath as well as any non-linearities that may arise with the inclusion of warm plasma effects. Although, as yet, no universally accepted model of the behavior of a space-based antenna exists, we note that our results can also be used with any other previously developed or future antenna-in-magnetoplasma model. We choose the *Wang and Bell* [1970] model for our work because it specifically addressed the VLF frequency range that we are interested in and presents results that encompass the magnetoplasma parameter ranges of interest.

The *Wang and Bell* [1970] model establishes two primary constraints on whistler-mode radiation with dipole antennas in the magnetosphere. Firstly, a short, electric dipole has a relatively small radiation resistance if the driving frequency is more than ~10% below the local f_{LHR}. Hence, a source located at the equator at $L = 2$ would not effectively radiate VLF waves below ~2.3 kHz -- which clearly indicates that our results presented above for 1-kHz waves should be properly qualified. Secondly, a VLF dipole antenna in a magnetoplasma emits the primary portion of its total radiated power as waves whose wavelength is approximately equal to the antenna length. In an anisotropic medium such as in the Earth's inner magnetosphere, wavelength is dependent on both wave frequency and direction with respect to the ambient magnetic field. For a given

location and wave frequency, the wavelength is uniquely determined by the wave normal angle. For antenna lengths of ~200-500 m and for the few kHz waves considered here, waves must have a wave normal angle within a few degrees of the resonance cone (or within a few degrees of $\psi = 90^o$ if $f < f_{LHR}$) in order to satisfy the requirement for the radiated wavelength to be approximately equal to the antenna length.

These above restrictions limit the allowable wave frequencies and the range of wave normal angles that can be used to direct the dispersal of whistler-mode wave energy. While in Figures 5, 6, and 7, we integrated and normalized over wave normal angles up to -75^o, the *Wang and Bell* [1970] theory suggests that there would be negligible radiated power beyond ~85^o. We, thus, expect that antenna radiation considerations, which limit effective radiation to only the most oblique wave normal angles, would then limit the *L*-shell range of illumination. To be consistent with the *Wang and Bell* [1970] model, we adjust the lower integration bound to be no more than three degrees away from the maximum wave normal angle considered (-89.9^o if $f < f_{LHR}$ or the resonance cone if $f > f_{LHR}$). Furthermore, we choose wave frequencies that are no lower than 90% of the local f_{LHR}.

This result of the inclusion of antenna radiation considerations is illustrated in Figure 9, which shows the effects of restriction of the wave normal angles and wave frequencies considered for rays injected from $L = 1.5$, $L = 2.0$ and $L = 2.5$ from both the geomagnetic equator and a latitude of 20^o along the field line. For each graph in Figure 9, we show the corresponding cavity enhancement factor for frequencies ~10% below, approximately equal to, and 1 kHz above the local f_{LHR}, with the frequencies chosen for each injection site given in Table 1. Additionally, for each wave frequency chosen, we have integrated and normalized over only the first three degrees in wave normal angle.

Table 1. The Wave Frequencies and Resonance Cone for the Six Different Injection Sites Considered Here.

Local Lower Hybrid Resonance Frequency

	$\lambda_s = 0^\circ$	$\lambda_s = 20^\circ$
$L = 1.5$	5.4 kHz	9 kHz
	6 kHz	10 kHz
	7 kHz	11 kHz
$L = 2.0$	2.3 kHz	3.8 kHz
	2.5 kHz	4.2 kHz
	3.5 kHz	5.2 kHz
$L = 2.5$	1.2 kHz	2.0 kHz
	1.3 kHz	2.2 kHz
	2.3 kHz	3.2 kHz

There are several important features of the results shown in Figure 9. As expected, the initial wave normal angle limitations necessitated by the *Wang and Bell*

[1970] model result in cavity enhancement over a smaller range of L-shells as compared to Figure 6. For instance, 2.5-kHz waves injected equatorially from $L = 2$, shown in white in the top middle graph of Figure 9, lead to relatively large cavity enhancement factors in the range $1.9 < L < 2.2$, whereas, including the full angular range (middle column, 2nd row in Figure 6) leads to large cavity enhancement factors up to $L \sim 2.4$. The requirement that the wave frequency be no smaller than ~90% of the local f_{LHR} also prevents the use of wave frequencies (generally 2-3 kHz below the local f_{LHR}) that would be suitable to target regions far from the injection site. This restraint is most evident for injections from $L = 1.5$, as shown in the left column of Figure 9, where the f_{LHR} at the geomagnetic equator and at a latitude of 20^o is 6 kHz and 10 kHz, respectively. The top panel, comparable to Figure 7, shows that restricting the angular and frequency range results in cavity enhancement only in the immediate vicinity of the transmitter location.

Waves radiated from $L = 1.5$ and a latitude of 20^o (refer to the bottom panel in the left column) are at such a high frequency — 9, 10, and 11 kHz — that no magnetospheric reflections occur for the model plasmasphere we have chosen. Sources this close to the Earth's surface can, therefore, be used to affect energetic electrons only on the first equatorial pass of the ray path, after which the ray energy is absorbed within the ionosphere. Another noteworthy feature is that the normalized, integrated cavity enhancement factor is larger when we integrate over only the first three degrees in wave normal space. Again, referring to 2.5-kHz waves injected equatorially from $L = 2$, we see that the cavity enhancement factor at $L = 2$ is ~3 when the full angular range is considered (middle panel in Figure 6) and ~10 for the smaller range (shown in green in the top, middle panel in Figure 9). This result is a consequence of the fact that rays with an initial wave normal almost perpendicular to the ambient magnetic field have much longer lifetimes than those with lower initial wave normal angles. Hence, integrating over a much broader range of wave normal angles does not add significantly to the cavity enhancement factor, and the small gain is then completely lost upon normalization over the number of injected rays. Thus, even though the *Wang and Bell* [1970] model greatly reduces the allowable angular range for wave normals, the most persistent (i.e., the most efficiently stored) rays are still retained and available for illumination of particular L-shell regions.

For the six source sites studied here ($L = 1.5$, 2.0, 2.5 and geomagnetic latitudes of 0^o, 20^o for each L-shell), a major overall conclusion is that only three sources, radiating power according to the *Wang and Bell* [1970] model, are required to project whistler-mode wave energy from $1.4 < L < 2.7$. The affected L-shell region displayed in Figure 9, in fact, represents a lower bound because we only investigated a single off-equatorial location. Simulating source locations at additional geomagnetic latitudes would necessarily increase the range of L-shells upon which significant cavity enhancement factors can be attained.

3.1.7. Summary: Cavity Illumination

We used the Stanford VLF ray-tracing code [*Inan and Bell*, 1977] coupled with an accurate estimation of the path-integrated Landau damping, combined with the data

set from *Bell et al.* [2002], to simulate a large number of whistler-mode wave frequencies and injection wave normal angles at six different magnetospheric source locations. By introducing the magnetospheric cavity enhancement factor, we quantitatively account for the fact that an ELF/VLF wave represented by a given injected ray, because of repeated reflections, may resonantly interact with energetic electrons multiple times during multiple equatorial crossings before its energy is diminished. At each equatorial crossing, the wave power is placed into L-bins and summation of the normalized power within each bin represents the cavity enhancement factor. Thus, a cavity enhancement greater than unity does not suggest amplification of wave power; instead, it simply reflects the fact that, due to a number of magnetospheric reflections, the total integrated normalized power projected (over time) at a single L-shell bin can be larger than unity.

The initial analysis involved first specifying an injection location, $L = 1.5$, $L = 2.0$, $L = 2.5$ and a geomagnetic latitude of 0^o and 20^o for each L-shell and, then, investigating the behavior of injected rays at wave frequencies from 1-10 kHz by 0.1 kHz. For each wave frequency, we studied initial wave normal angles from -75^o up to -90^o. Examination of the results of these simulations has allowed us to assess the feasibility of projection of wave energy on particular L-shell ranges in the inner radiation belts. In general, waves settle on L-shells where the wave frequency is approximately equal to the lower hybrid resonance frequency at the geomagnetic equator on that L-shell. Thus, waves with frequencies below the local f_{LHR} move outwards from the injection site and wave frequencies above the f_{LHR} move inwards. The injection wave normal angle further determines the behavior of the ray path, with rays having wave normal angles initially more perpendicular (parallel) staying closer to (dispersing farther from) the injection L-shell.

The inclusion of Landau damping in our results provides an accurate picture of where the largest cavity enhancement factors occur. Frequencies below the local f_{LHR} and waves with an initial perpendicular normal angle persist for a much longer time (up to ~60 seconds in some cases) than waves with frequencies above f_{LHR}. Consequently, minimal cavity enhancement factors occur at L-shells inwards from the injection site because the high frequency waves that would be used to target those locations are also the waves that experience the strongest Landau damping. Additionally, for off-equatorial injections, while damping occurs more quickly than equatorial injections, resulting cavity enhancement factors can be significant over a broader range of L-shells. These initial results indicate that, before antenna radiation pattern is considered, only 3 sources are needed to illuminate the region of $1.3 < L < 3.5$ with relatively large cavity enhancement factors.

We also investigated the effects that the use of a practical transmitting antenna in the magnetosphere would impose on our simulations, with the most applicable theory in this connection being the *Wang and Bell* [1970] model of a short, electric dipole radiating in a magnetized plasma. The two primary limitations imposed by this theory are constraints on the driving frequency and initial wave normal angle. According to the Wang and Bell [1970] theory, wave frequencies below ~90% of the local f_{LHR} or initial wave normal angles beyond $\sim 3^o$ of the resonance cone contain negligible radiated

power. Thus, for each source location, we repeated our analyses for a restricted range of wave frequencies and injection wave normal angles.

In conclusion, our results indicate that, even after incorporation of the limitations resulting from the Wang and Bell [1970] model, only three sources, in orbit and, thus, radiating alternately at both equatorial and off-equatorial sites at $L = 1.5$, $L = 2.0$, and $L = 2.5$, and utilizing driving frequencies no lower than ~90% of the local f_{LHR}, are needed to illuminate (with significant cavity enhancement factors) the L-shell range of $1.4 < L < 2.7$. Given that only two geomagnetic latitudes were studied, this L-shell range — already comprising the bulk of the inner radiation belts — represents a lower limit to which we can project whistler-mode wave energy. Additional minor changes to the results shown might come about with the inclusion of ray paths outside of the meridional plane, as would be possible with a three-dimensional ray tracer. With initial wave normals outside the meridional plane, there would be differences in the deposition of whistler-mode wave energy, although we do not expect any substantial changes to our conclusions. *Cair'o and Lefeuvre* [1986] have used three-dimensional ray tracing to study the propagation of ELF/VLF hiss in the magnetosphere. Their study indicates that highly oblique whistler waves (with initial wave normal angles in the range considered in this study) tend to see an azimuthal angle approximately constant in the course of their propagation.

Thus far, our work has addressed topics 1, 2, 3, and 5 discussed in the Introduction. We, now, turn to the energetic electron precipitation that would be caused by space-based ELF/VLF transmitters, thereby, addressing topic 4 discussed in the Introduction.

3.1.8. Energetic Electron Precipitation

The results of both *Inan et al.* [2003] and *Kulkarni et al.* [2006] laid the groundwork to determine whether in-situ injection is a feasible means of achieving controlled precipitation of energetic electrons. The former paper highlighted the higher diffusion coefficients and long lifetimes of low frequency magnetospherically reflecting (MR) whistler-mode waves. The latter identified specific locations and operating frequencies that would be utilized if such a scheme were to be implemented. However, neither study determined the precipitation signatures that would be induced by a space-based source.

In this connection, it is important to note that *Inan et al*. [2003] calculated diffusion coefficients for waves at a constant wave normal angle, ψ, of 45^o. Magnetospherically reflecting whistler mode waves, on the other hand, propagate obliquely with ψ near the resonance cone at an angle near 90^o (see below). Therefore, the diffusion coefficients presented by *Inan et al*. [2003] may not apply to waves injected from an in-situ source if these waves have reflected one or more times. If high wave normal angles result in small diffusion coefficients — a result implied by both *Inan et al*. [2003] and *Inan and Bell* [1991] — the benefit of multiple reflections may be lost. *Inan et al*. [2003] recognized, but left unresolved, this issue, which we address here. We use the Stanford VLF Ray Tracing Program [*Inan and Bell*, 1977], calculate path-integrated

Landau damping and determine the precipitation signatures [*Bortnik et al*., 2006b] that would be induced by an in-situ source located in the inner radiation belts.

3.1.9. Simulation Procedure

To calculate the energetic (>100 keV) electron precipitation induced by in-situ VLF transmitters, we incorporate three separate models: (1) radiation pattern of an antenna immersed in a magnetoplasma, (2) ray paths within the magnetosphere, which depend on magnetic field and particle density models, and (3) resonance interaction between energetic electrons and VLF waves, which induce precipitation based on an assumed electron phase space velocity distribution function and loss-cone pitch-angle distribution. The first two models have been described above, and so we focus on the third model here.

In this study, we launch rays for a half-second pulse from four locations: $L = 2$ and $L = 2.5$ at the equator and a geomagnetic latitude of 20^o for each L-shell. Although *Kulkarni et al*. [2006] also considered $L = 1.5$, we neglect that site because the required operating frequencies are too high for magnetospheric reflections to occur. At each source site, we select three wave frequencies as described above. Then, for each frequency, we launch 30 rays separated by 0.1^o in wave normal angle, starting at the resonance cone. We consider a 1-W transmitter and divide this power equally among the rays, assuming that the wave k-vectors are primarily directed along the resonance cone [*Wang and Bell*, 1972]. We determine the latitudinal and azimuthal ($\pm 3^o$) spread of the rays at 1 km, and ultimately assign each ray an initial Poynting flux of 1e-9 [W/m^2]. However, because we are interested in signatures, rather than predicting the amount of induced precipitation, our analysis and results are insensitive to the specific value chosen. Because we use a 2D ray tracer, we can only trace rays within the meridional rays and our results therefore represent a lower limit on the induced precipitation.

As the rays propagate, they interact with, and precipitate, energetic electrons. We use the methodology described in *Bortnik et al*. [2006a], which integrates the equations in *Bell* [1984], for resonance modes, m, from $-5 \leq m \leq 5$ to calculate the pitch-angle change induced by in-situ sources considered here. To determine the flux of precipitated particles, we apply the calculated pitch-angle change to loss-cone electrons. This procedure allows us to determine the induced precipitation signatures that would be observed at 100-km altitude at a range of L-shells around the source [*Bortnik et al*., 2006b].

The AE8 distribution for trapped energetic electrons, with an assumed sinusoidal loss cone pitch-angle distribution, exhibits a sharp dropoff in flux levels with increasing energy [*Vette*, 1991]. While this model would yield more realistic electron precipitation signatures, it obscures the potential efficacy of MR waves at inducing >1-MeV precipitation. The signatures that result from using the AE8 radiation belt model (Figure 11) show large fluxes of <100-keV electons, and relatively weak fluxes of >1-MeV electrons. These results prevent us from determining if MR whistler-mode waves are

ineffective at scattering > 1-MeV electrons, or if there are simply too few electrons at those energies to precipitate. We, therefore, assume a constant flux of 50,000 cm^{-2}-s^{-1}-$ster^{-1}$-keV^{-1} for all electron energies up to 5 MeV, with a square loss cone pitch-angle distribution. The numerical value is approximately equal to the 100-keV flux at $L = 2$ in the AE8 model. Using this somewhat contrived distribution function allows us to make meaningful comparisons between >1-MeV and <1-MeV precipitation. Our results would be somewhat more accurate, however, in the aftermath of geomagnetic storms where the radiation belts are filled with large fluxes of >1-MeV electrons.

3.1.10. Wave-Particle Interaction and Electron Precipitation

MR whistler-mode waves generally propagate with wave normal angles very close to the resonance cone [*Jasna et al*., 1990]. Waves with highly oblique wave normal angles from 85^{o}-90^{o} induce different precipitation signatures than waves with smaller values of ψ. We can plot, similar to Figure 4 in *Jasna et al*. [1990], $Y = \psi - \psi_{res}$, where ψ is the wave normal angle along the raypath. Figure 10 shows Y along the ray path for waves injected from $L = 2$ at the equator. We show wave frequencies of 1, 2.5, and 4 kHz, and initial wave normal angles of $\psi = -85^{o}$, -45^{o}, and 0^{o}. Note that, regardless of operating frequency, initial wave normal angle, or whether the frequency is below or above the local f_{LHR}, ψ approaches the resonance cone ($Y \sim 1^{o}$) within 10 seconds. Wave frequencies just below or above the local f_{LHR}, ~ 2.5 kHz, approach the resonance cone even more quickly.

This last point affects the feasibility of using in-situ injection to precipitate energetic electrons. *Kulkarni et al*. [2006] suggested that the restricted initial wave normal angles implied by the *Wang and Bell* [1970] model limited the region of illumination. While this statement is true, a bigger factor may be the scattering efficiency. Even a new technology that effectively radiates at low wave normal angles of, e.g., 45^{o}, would not change the propagation characteristics in a cold, smooth magnetoplasma. Within two to three magnetospheric reflections, all waves are very close to the resonance cone regardless of wave frequency or initial ψ. Thus, in the cold, smooth magnetoplasma considered here, all MR whistler-mode waves will very quickly have wave normal angles close to the resonance cone. Again, *Inan et al*. [2003] suggested that high wave normal angles might negatively impact scattering efficiency but did not resolve the issue.

Bell [1984] gives the gyro-averaged equations of motion for the resonance interaction between an obliquely propagating whistler-mode wave and an energetic electron for a general harmonic resonance m:

$$\frac{d\alpha}{dt} = -\frac{\omega_{tm}^2}{k_z v_{perp}}\left(1 + \frac{\omega \cos^2\alpha}{m\omega_H - \omega}\right)\sin\eta + \frac{v_{perp}}{2\gamma\omega_H}\frac{\partial\omega_H}{\partial z} \qquad (1)$$

where $\omega_{\tau m}^2 = (-1)^{m-1}\,\omega_{\tau 0}^2\,[J_{m-1}(\beta) - \alpha_1 J_{m+1}(\beta) + \gamma\alpha_2 J_m(\beta)]$, $\omega_{\tau 0}^2 = (\omega_1 k_z p_{perp}/\gamma m_e)$, $\omega_1 = (e/2m_e)(B_x + B_y)$, $\omega_2 = (e/2m_e)(B_x - B_y)$, $\alpha_1 = (\omega_2/\omega_1)$, $\alpha_1 = (eE_z/\omega_1 p_{per})$, $\beta = (k_x p_{perp}/m_e\gamma\omega_H)$, $\gamma = 1/(1 - v^2/c^2)^{1/2}$, $k_z = k\cos\psi = (\omega\mu/c)\cos\psi$, $k_x = k\sin\psi$, where k is the wave k-vector, μ is the refractive index, J_i are Bessel functions of the first kind of order i, v_{perp} is the component of the electron velocity perpendicular to the ambient magnetic field, ψ is measured with respect to the ambient magnetic field assumed to be in the z-direction, B_x, B_y, E_z are the magnetic and electric field components of the whistler-mode wave, η is the phase between the right hand component of the wave magnetic field and v_{perp}, and ω_H is the electron gyrofrequency.

This equation shows that the electron pitch-angle changes as a result of both wave forces which occur during the wave-particle interaction, and adiabatic variation. In principle, an electron would be trapped indefinitely on a given field line in the absence of wave forces [*Walt*, p. 42]. Only wave forces, however, can induce a change in the electron equatorial pitch angle which otherwise remains constant during adiabatic motion. Wave-induced pitch-angle change accumulates only when the phase angle η remains constant for extended periods. This restriction implies that $d\eta/dt = 0$, which leads to the resonance condition between an energetic electron and a whistler-mode wave:

$$v_z = \frac{m\omega_H/\gamma - \omega}{k_z} = \frac{m\omega_H/\gamma - \omega}{\omega\mu\cos\psi}c \qquad (2)$$

where v_z is the resonant electron velocity along the Earth's magnetic field, m, an integer, is the resonant mode, and the remaining terms have been defined above [*Bell*, 1984].

We now highlight relevant features of the above two equations, starting with Equation 2. This equation shows how location (which affects ω_H) and ω affect resonant velocity: v_z is inversely proportional to ω and directly proportional to ω_H if k_z is constant. Moreover, as the absolute value of m increases, the resonant energy increases. Non-zero m indicates a perpendicular or cyclotron resonance between the wave magnetic field and electron, while $m = 0$ represents the Landau resonance. See Figure 12 for plots of resonant electron energy, for $m = 1$, along the ray path. Note that resonant energy, E_{res}, increases off the equator because ω_H increases off the equator (a similar plot was also shown in *Jasna et al*. [1990]). The low wave frequencies of 1-5 kHz injected from an in situ source always undergo cyclotron resonance with electrons of energies >100 keV, and often resonate with >1-MeV electrons. Note that, as ψ increases, $k_z = \omega\mu\cos\psi/c$ decreases, if everything else is constant. Smaller k_z, in turn, leads to higher parallel resonant energies, as shown in Equation 2. Thus, a wave propagating at, e.g., $\psi = 45^o$, will generally resonate with lower energy electrons than a wave propagating at $\psi = 85^o$. These high resonant electron energies, along with long lifetimes due to magnetospheric reflections, are why *Inan et al*. [2003] suggested in-situ injection could be a promising means of achieving controlled precipitation.

As an MR whistler-mode propagates, it resonates with, and pitch-angle scatters, energetic electrons at all points along its path. However, the inhomogeneity of the

Earth's magnetic field plays a dominant role in determining the wave-particle interaction time (or the duration of the resonant scattering). Slower variation of magnetic field amplitude, which occurs at the equator, allows the wave-particle interaction to endure for a longer time and, thus, often dominates the precipitation signature [\textit{Inan et al.}, 1982]. Also note that several terms in Equation 1 depend on the wave normal angle, ψ, between the wave k-vector and $\mathbf{B}_0$. The wave normal angle can play a crucial role in determining the precipitation signatures induced by an in-situ source. *Inan et al*. [2003] noted that high wave normal angles are associated with decreased pitch-angle scattering, which might decrease the efficacy of an in-situ source.

To summarize, MR whistler-mode waves undergo cyclotron resonance with >100- keV and >1-MeV electrons along their path. Pitch-angle scattering, however, is most effective near the magnetic equator and partially depends on the wave-normal angle ψ. The k-vector of an MR whistler-mode wave stays very close to ψ_{res} during its ray path, which results in a very large electron resonant velocity and also affects pitch-angle scattering efficiency.

We now return to the primary question raised in *Inan et al*. [2003] regarding the feasibility of in-situ injection to achieve controlled precipitation: Do the benefits of high resonant energies and long lifetimes due to magnetospheric reflections outweigh the possible reduced pitch-angle scattering associated with wave normal angles close to the resonance cone? We must highlight that in their study, *Inan et al*. [2003] calculated diffusion coefficients and resonant wave frequencies for 1.5-MeV and 3-MeV electrons versus ψ at a single equatorial location. *Albert* [1999] kept ψ constant and calculated resonant frequencies. The precipitation induced by an in-situ source, however, results from a different process: the frequency is fixed, ψ changes along the ray path and the wave undergoes both cyclotron and Landau resonance, at different points in space, with electrons from ~10 keV to > 1 MeV.

Because plasma and wave parameters, such as ω_H and μ, are constantly changing along the ray path, we should not extrapolate the total >1-MeV precipitation induced by MR whistler-mode waves from the diffusion coefficients of 1.5-MeV electrons calculated at a single location. In fact, as our simulation results show, waves injected at ψ close to ψ_{res} can induce more >1-MeV precipitation than waves injected parallel to $\mathbf{B_0}$.

3.1.11. Simulation Results and Analysis

Figure 11 displays differential number flux at 100-km altitude induced by an equatorial source at $L = 2$. We show the precipitation signatures that would be observed in the northern and southern hemispheres at 100-km altitude at a range of L-shells around the source. These results show the combined effect of including resonance modes $-5 \leq m \leq 5$, and both equatorial and off-equatorial interactions. In this figure alone, we use the AE8 radiation belt for the trapped radiation fluxes.

The f_{LHR} at $L = 2$ at the equator is ~2.5 kHz. Note, first, that 2.3-kHz waves propagate outwards to $L \sim 2.1$ and persist for more than 20 seconds. The precipitation

signature induced by 3.5-kHz waves, on the other hand, moves inwards to $L = 1.9$ and the waves induce precipitation for a much shorter period of time. The quasi-periodicity you see in all the panels is a result of the interaction occurring primarily near the equator. Because the waves magnetospherically reflect, we observe precipitation bursts roughly on the period that it takes the wave to reach the equator. Second, note that there are large, intense precipitation peaks <100 keV, and very weak, sometimes barely visible, precipitation bursts ~>1 MeV. The former peaks are the result of the Landau resonance, and the latter case is controlled by cyclotron resonance. Because these two interactions occur by different physical mechanisms, certain electron energies often do not resonate with a given wave. Furthermore, there are many more electrons at lower energies and, thus, the differential number flux will be more intense.

For the remainder of this study, we use the constant distribution function described above. We wish to quantify how much additional >100-keV and >1-MeV precipitation is gained from the MR process. To that end, we calculate the number of energetic electrons precipitated before and after the first magnetospheric reflection. To be consistent with *Inan et al*. [2003], we denote this parameter the cavity gain factor. In this study, however, the gain represents additional precipitation, not solely equatorial crossings. We then compare the cavity gain factor for all the wave frequencies and source locations considered here.

Figure 13 shows the differential number flux, in the northern hemisphere, induced by a 3.5-kHz equatorial source at $L = 2$. These calculations used a constant distribution function of 50,000 cm^{-2}- s^{-1}-$ster^{-1}$-keV^{-1} with a square loss-cone. Thus, the results greatly underestimate the <100-keV electron precipitation (see Figure 11 for a more realistic precipitation signature). Compared to Figure 3, the >1-MeV precipitation signature in Figure 13 is much stronger relative to the <1-MeV precipitation. In fact, during the first 3-4 reflections, precipitation for electrons both above and below 1 MeV is approximately equal. As the wave settles at $L = 1.9$ after several reflections, the precipitation signature for >1-MeV electrons is 2-3 orders of magnitude weaker than for <1-MeV electrons. In Figure 11, the >1-MeV precipitation signature is approximately 8 orders of magnitude lower at all times. Those substantially weaker signatures, therefore, result from the AE8 distribution, which contains relatively few energetic electrons, rather than the presumed inefficient scattering induced by MR whistler-mode waves. Figure 13 shows that MR whistler-mode waves propagating at high wave normal angles can precipitate >1-MeV electrons much more effectively than would be believed by examining the flux derived from the AE8 radiation belt mode. Moreover, MR whistler-mode waves resonate with much higher energy electrons because large ψ increases resonant electron velocity through smaller k_z (see discussion above). Even if ψ extremely close (<~0.5°) to ψ_{res}, which occurs after the first few reflections, decreases scattering efficiency, the much larger resonant electron energies appear to somewhat compensate in the >1-MeV precipitation signature.

Table 2 shows the cavity gain factors for >100 keV and >1 MeV at all the source locations and frequencies considered here. We include the total number of precipitated electrons in both the northern and southern hemisphere. We should reiterate that these

numerical results are based on a constant energetic electron distribution function. The relevant trends can be explained as follows: At each source site, except for an equatorial source at $L = 2$, higher wave frequencies induce less precipitation because of shorter lifetimes. At the equator at $L = 2$, however, 2.3-kHz and 2.5-kHz waves, along their ray paths, undergo cyclotron resonance primarily with >5 MeV. Thus, the total induced precipitation is relatively low because our energetic electron distribution contains no electrons >5 MeV in energy. For all source sites, the cavity gain factor decreases with frequency due to, again, shorter lifetimes, which leads to fewer magnetospheric reflections. For 3.5-kHz waves, e.g., there is relatively less precipitation induced after the first pass than for 2.5-kHz waves. Off-equatorial sources induce stronger precipitation signatures because resonance energy increases at higher latitudes, and the longer ray paths, therefore, resonate with more energetic electrons. The decreased scattering efficiency at higher latitudes [*Inan et al*., 1981] appears to be less important than high resonant energy. Finally, the stronger precipitation signatures at $L = 2.5$, compared to $L = 2$, occur because waves injected from that source site have longer lifetimes (not shown). In all cases, multiple magnetospheric reflections lead to precipitation several times more >1-MeV electrons as compared to a single pass interaction. These results demonstrate that the MR whistler mode waves that would be injected from in-situ sources may be effective at controlled precipitation of energetic electrons.

Table 2. The Number of Precipitated Electrons and Cavity Gain Factors.

		Number of Precipitated Electrons		Cavity Gain Factor	
		> 100 keV	> 1 MeV	> 100 keV	> 1 MeV
$L = 2$, $\lambda = 0°$	2.3 kHz	1.57	1.57	16.1	16.1
	2.5 kHz	1.89	1.89	15.9	15.9
	3.5 kHz	2.20	2.18	10.5	10.5
$L = 2$, $\lambda = 20°$	3.8 kHz	4.37	4.24	14.5	14.1
	4.2 kHz	3.47	3.32	10.7	10.2
	5.2 kHz	2.33	2.10	5.6	5.4
$L = 2.5$, $\lambda = 0°$	1.2 kHz	8.96	8.91	10.8	10.7
	1.3 kHz	8.61	8.52	9.4	9.4
	2.3 kHz	5.65	4.29	4.2	5.3
$L = 2.5$, $\lambda = 20°$	2.0 kHz	16.76	13.98	6.9	6.3
	2.2 kHz	14.56	11.65	6.1	5.8
	3.2 kHz	6.93	4.85	2.8	3.1

Figures 14 and 15 show the precipitation and illumination spectra for the source sites and frequencies discussed. Note that waves with frequencies below (above) the local equatorial f_{LHR} precipitate electrons primarily at L-shells higher (lower) than the source location. Also note that off-equatorial sources induce stronger >1-MeV precipitation signatures, and that higher frequencies generally induce weaker ones. The exception for an equatorial source at $L = 2$ was explained above. In this case, Figure 14 shows that 2.3-kHz and 2.5-kHz waves only precipitate 3- to 5-MeV electrons, while 3.5-kHz waves resonate with electrons energies down to 2 MeV.

The results shown, thus far, were all based on sources radiating waves close to the local f_{LHR} and injected at initial wave normal angles very close to the resonance cone. Such waves tend to remain close to the source site and settle on an L-shell very quickly. Furthermore, such waves tend to persist for 15 to 20 seconds before being Landau damped by 10 dB. Waves injected with less oblique wave normal angles, on the other hand, propagate much farther from the source and have relatively short lifetimes [*Kulkarni et al*., 2006]. Although we have restricted the initial wave normal angle, it would still be instructive to compare the precipitation induced by waves with lower initial ψ with our previous calculations. These results would be useful in the event that a longer antenna is used to effectively radiate at initial ψ far from the resonance cone.

Figures 16a and 16c show two 3.5-kHz rays injected, at initial ψ of -88^o (ray 1) and -45^o (ray 2), from the geomagnetic equator at $L = 2$. The middle row shows the Landau damping along the ray path for these two rays. There are several relevant features that we must highlight. Note that, ray 1 stays very close to the source L-shell, persists for ~15 seconds, and magnetospherically reflects several (17) times very close to the geomagnetic equator. In fact, the ray stays within $\pm 10^o$ of the equatorial region. Ray 2, on the other hand, propagates up to $L \sim 3$, is Landau damped by 10 dB within 10 seconds, magnetospherically reflects only 7 times, and propagates up to a geomagnetic latitude of $\sim 30^o$. Shorter lifetimes and fewer magnetospheric reflections imply that waves injected at lower initial ψ will precipitate fewer energetic electrons as compared to the results shown earlier. Moreover, waves injected at low initial ψ (e.g., ray 2) propagate up to very high geomagnetic latitudes where pitch-angle scattering is relatively inefficient [*Inan et al*., 1982].

Table 3 compares the >100 -keV and >1-MeV electron precipitation induced by a 3.5 kHz equatorial source at $L = 2$. We followed an identical procedure, as described above, but considered 30 rays centered at 0^o, -25^o, -45^o and -65^o instead of near the resonance cone. For reference, the last row reproduces the results shown in Table 2, where the rays were injected within 3^o of ψ_{res}. Note that waves injected at less oblique initial wave normal angles generally precipitate fewer >1-MeV electrons. The >100-keV precipitation signature, however, is stronger when the initial wave normal angle is closer to $\mathbf{B_0}$ because the larger k_z leads to lower resonant energies than waves with ψ close to ψ_{res}. Although such waves are less effective at inducing >1-MeV electron precipitation, they do precipitate electrons at a broader range of L-shells. Figure 17 shows the precipitation and illumination spectra for the range of initial wave normal angles just described. Note that the signature is generally stronger at lower energies, and that increasing ψ leads to illumination over a narrower range of L-shells. For waves injected at $\psi \sim 0^o$, the ray paths are such that certain L-shells are not illuminated with whistler-mode wave energy (see Figure 16b).

Our results indicate that MR whistler-mode waves injected at high initial wave normal angles from an in situ source may be more effective than previously thought at inducing >1-MeV electron precipitation [*Inan et al*., 2003]. Compared to a single-pass interaction, multiple reflections sometimes induce more than an order of magnitude more

energetic electron precipitation. However, only locations within ~0.1L of the source site can be effectively targeted. Projecting whistler-mode wave energy to more distant L-shells would require injecting high power waves at low (<~ 45^o) initial wave normal angles, which does not appear possible at antenna lengths of a few hundred meters. Even if that were possible, such waves are Landau damped very quickly and induce less >1 MeV precipitation. These two conclusions together imply that illuminating a broad region of the magnetosphere may require several sources distributed radially. Further investigation is required to determine if three-dimensional ray tracing, warm plasma effects or the existence of density irregularities would change this result.

Table 3. The Number of Precipitated Electrons and Cavity Gain Factors for Different Initial Wave Normal Angles for a 3.5-kHz Equatorial Source at L = 2.

	Number of Precipitated Electrons		Cavity Gain Factor	
	> 100 keV	> 1 MeV	> 100 keV	> 1 MeV
0°	2.38	1.09	14.6	21.7
25°	3.90	1.32	32.4	80.7
45°	1.83	0.73	18.3	51.0
65°	2.94	2.06	21.4	51.4
~ 87°	2.20	2.18	10.5	10.5

3.1.12. Conclusion

We have calculated precipitation signatures for four different in situ sources located at L = 2.0, 2.5, at the geomagnetic equator and a latitude of 20^o. We incorporated the *Wang and Bell* [1970] model for a short, electric dipole immersed in a magnetoplasma to restrict both the operating frequency and initial wave normal angle of the injected rays. At each source site, we selected three operating frequencies around the local lower hybrid resonance frequency, f_{LHR}: 0.90 f_{LHR}, ~f_{LHR}, and f_{LHR} + 1 kHz. For each wave frequency, we launched 30 rays from the resonance cone, ψ_{res}, to ψ_{res} + 3^o. We used the Stanford VLF Ray Tracing Program [*Inan and Bell*, 1977] to calculate ray paths based on a simple dipole model for the Earth's magnetic field and the *Carpenter and Anderson* [1992] model for the particle density. We incorporated the effects of Landau damping along the ray path, and used the velocity space distribution function specified in *Bell et al*. [2002]. The results of the ray tracing and Landau damping calculation were then used to determine the induced energetic electron precipitation based on the methodology described in *Bortnik et al*. [2006a].

In a cold, smooth magnetoplasma, magnetospherically reflecting (MR) whistler-mode waves, after a few reflections, propagate at wave normal angles very close to ψ_{res}. This outcome is relatively insensitive to operating frequency or initial ψ. As they propagate, MR whistler-mode waves undergo both Landau and cyclotron resonance with electrons in the Earth's radiation belts. The Landau resonant particles are <100 keV and,

mostly, <10 keV. Cyclotron resonance occurs with >100-keV electrons, and resonant energies can be as high as a few MeV. The wave-particle interaction is most effective near the geomagnetic equator because the slow variation of the Earth's magnetic field allows for the longest interaction time.

We have defined the cavity gain factor, a ratio of total electrons precipitated to the number precipitated before the first reflection. Calculating the cavity gain factor for the different source location and operating frequency configurations show that, compared to a single-pass interaction, MR whistler-mode waves induce substantial >100-keV and >1- MeV electron precipitation. Equatorial sources radiating just below or at the local f_{LHR} induce the most >1-MeV precipitation, and off-equatorial sources induce the least. These results indicate that an in-situ source radiating waves close to the local f_{LHR} at high initial wave normal angles may be effective at inducing controlled precipitation of energetic electrons. We also determined the precipitation that would be induced by sources radiating waves at much lower initial ψ. Waves injected at lower initial wave normal angles are damped more quickly, undergo fewer magnetospheric reflections, and propagate up to high latitudes where pitch-angle scattering is relatively inefficient [*Inan et al*., 1982]. A source that could radiate at low initial ψ would, therefore, be less effective than one that injects waves at ψ close to ψ_{res}.

Future studies should determine the effect of including three-dimensional ray tracing, a warm plasma analysis, and magnetic-field density irregularities. The work of *Hashimoto et al*. [1977], for example, indicates that the effects of the resonance cone may be moderated if we include a nonzero particle temperature, and might modify the results shown here.

(Blank Page)

PUBLICATIONS AND PRESENTATIONS

The results of work supported under F19628-03-C-0059 have been published in peer reviewed scientific journals and presented at scientific conferences. These are listed below.

PUBLICATIONS

1. Kulkarni, P., U. S. Inan, T.F. Bell and J. Bortnik (2007), Precipitation signatures of ground-based VLF transmitters, J. Geophys. Res., (submitted)

2. Inan, U. S., M. Golkowski, M. K. Casey, R. C. Moore, W. Peter, P. Kulkarni, P. Kossey, E. Kennedy, (2007) Subionospheric VLF Observations of Transmitter-Induced Precipitation of Inner Radiation Belt Electrons, Geophys. Res. Lett.*,, 34*, L02106, doi:10.1029/2006GL028494.

3. Kulkarni, P., U. S. Inan, and T. F. Bell (2006), Whistler mode illumination of the plasmaspheric resonant cavity via in situ injection of ELF/VLF waves, *J. Geophys. Res.*, 111, A10215, doi:10.1029/2006JA011654.

4. Bell, T.F., U. S. Inan, T. Chevalier (2006), Current distribution of a VLF electric dipole antenna in the plasmasphere, Radio Sci., 41, RS2009, doi:10.1029/2005RS003260.

CONFERENCE PRESENTATIONS

1. Kulkarni, P., Inan, U.S., Bell, T.F., Bortnik, J., Precipitation Signatures of Ground Based VLF Transmitters, Presented at 8th International School/Symposium for Space Simulations, February 2007.

2. Kulkarni, P., Inan, U.S., Bell, T.F., In-situ and Ground-Based Illumination of the Inner Radiation Belts with Whistler-Mode Wave Energy, Presented at U.S. National Committee of the International Union of Radio Science, January 2006.

3. Kulkarni, P., Inan, U.S., Bell, T.F., Precipitated Fluxes of Radiation Belt Electrons via Injection of Whistler-Mode Waves, Poster SM41A-1175 presented at American Geophysical Union Fall Meeting, December 2005. (This poster won an Outstanding Student Paper award)

4. Kulkarni, P., Inan, U.S., Bell, T.F., Energetic Electron Precipitation via in-situ Injection of ELF/VLF Waves, Presented at International Union of Radio Science General Assembly, October 2005.

5. Kulkarni, P., Inan, U.S., Bell, T.F., Whistler Wave Illumination of the Plasmaspheric Cavity via in-situ Injection of ELF/VLF Waves, Presented at U.S. National Committee of the International Union of Radio Science, January 2005.

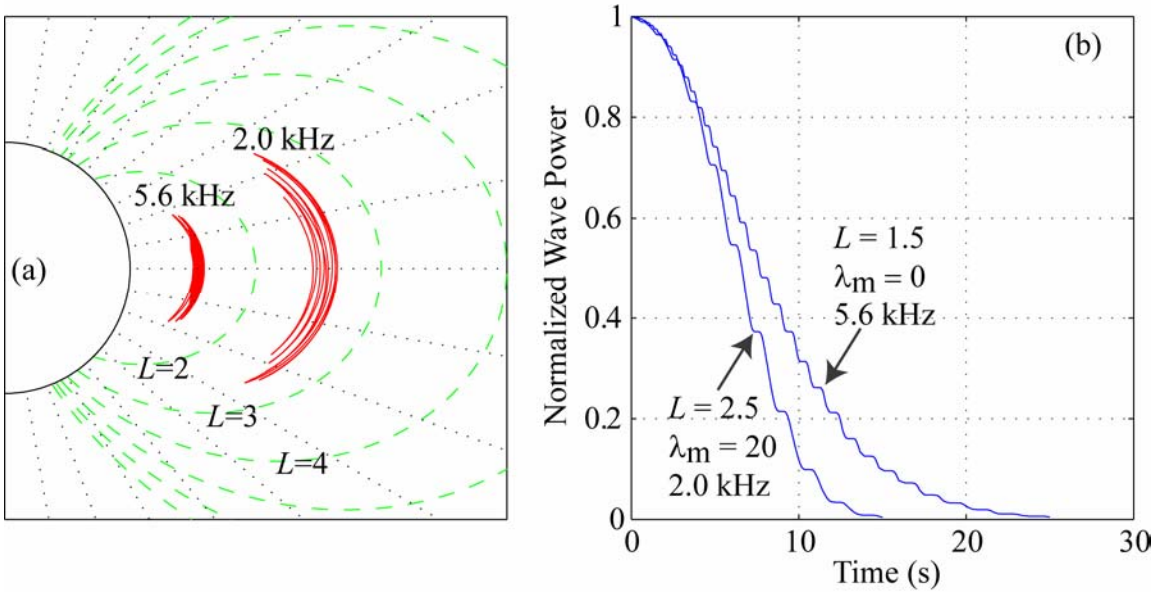

Figure 1: (a) Ray paths of a 5.6- kHz signal injected at $L = 1.5$ at the equator and a 2.0- kHz signal injected at $L = 2.5$ and $\lambda = 20^{o}$. (b) Variations of the wave power density along the ray paths at different L-shells.

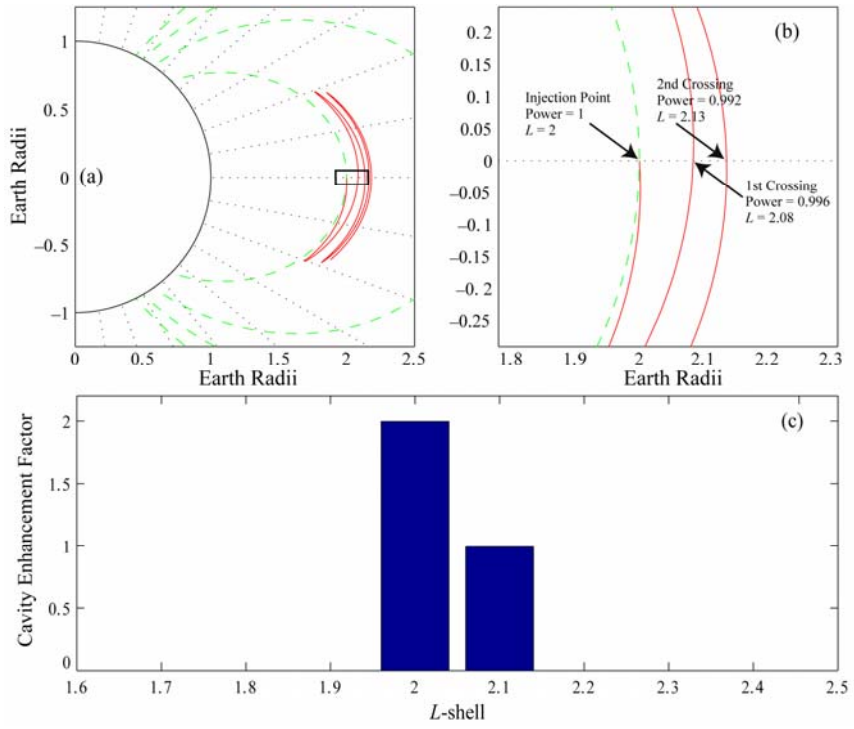

Figure 2: (a) Ray path of a 2.5- kHz signal injected at the geomagnetic equator at $L = 2$ with an initial wave normal angle of -85^{o}. (b) An expanded portion from the ray path shown in (a). (c) The cavity enhancement factor after signal injection plus the first two equatorial crossings.

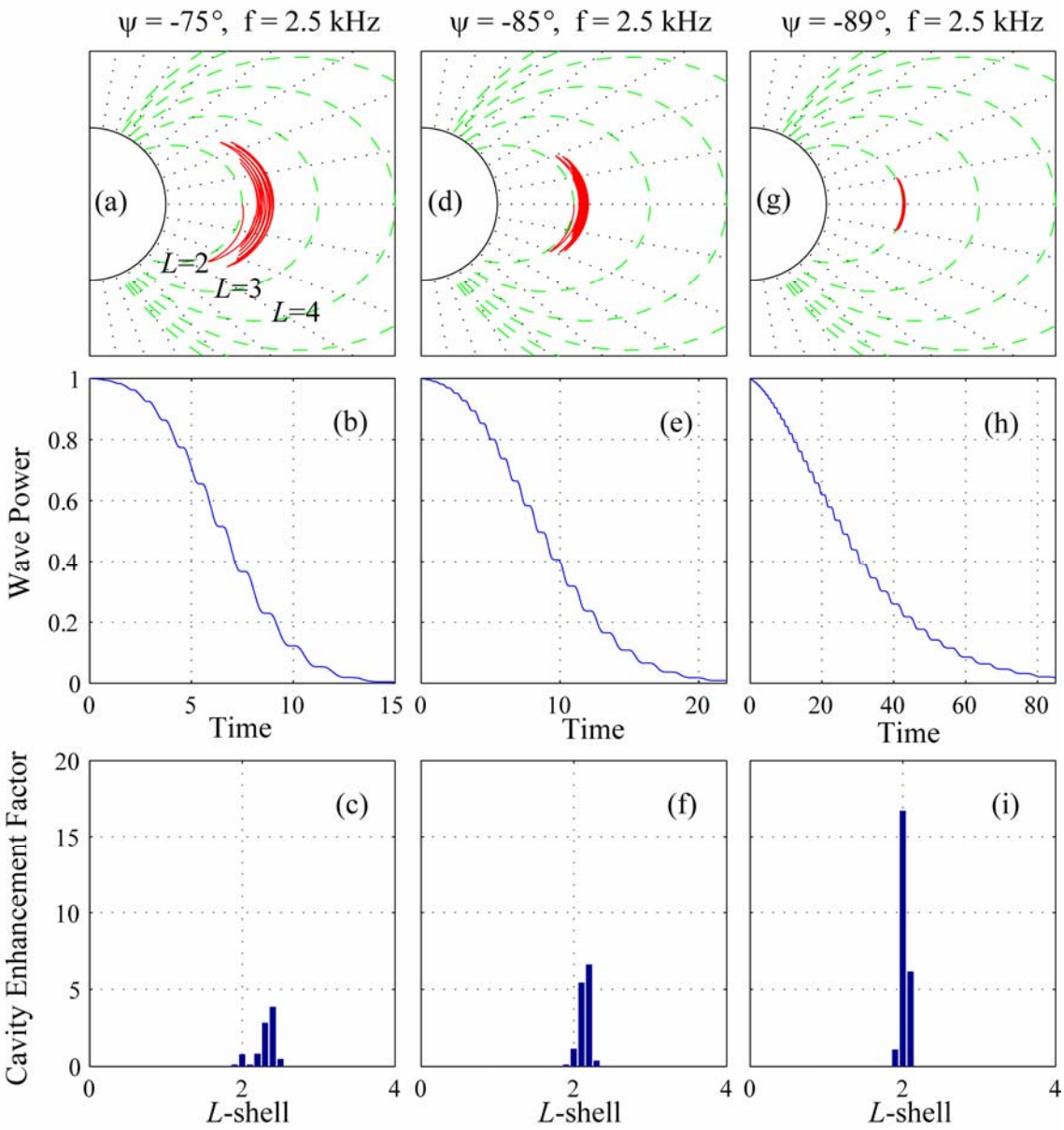

Figure 3: (a) Ray path of a 2.5-kHz (~ local f_{LHR}) signal injected at the equator at L = 2 at a wave normal angle of -75°. (b) Normalized wave power along the ray path. (c) Cavity enhancement factor at the equator as a function of L-shell. (d) Ray path for a wave injected at a wave normal angle of -85°. (e) Wave energy persists for a longer time when the injection wave normal increases. (f) Cavity enhancement also increases when the injection wave normal angle increases. (g) An almost perpendicular injection wave normal angle almost results in numerous magnetospheric reflections near the L = 2 shell. (h) This signal persists for many tens of seconds. (i) The cavity enhancement factor is even larger with an injection wave normal angle of -89°.

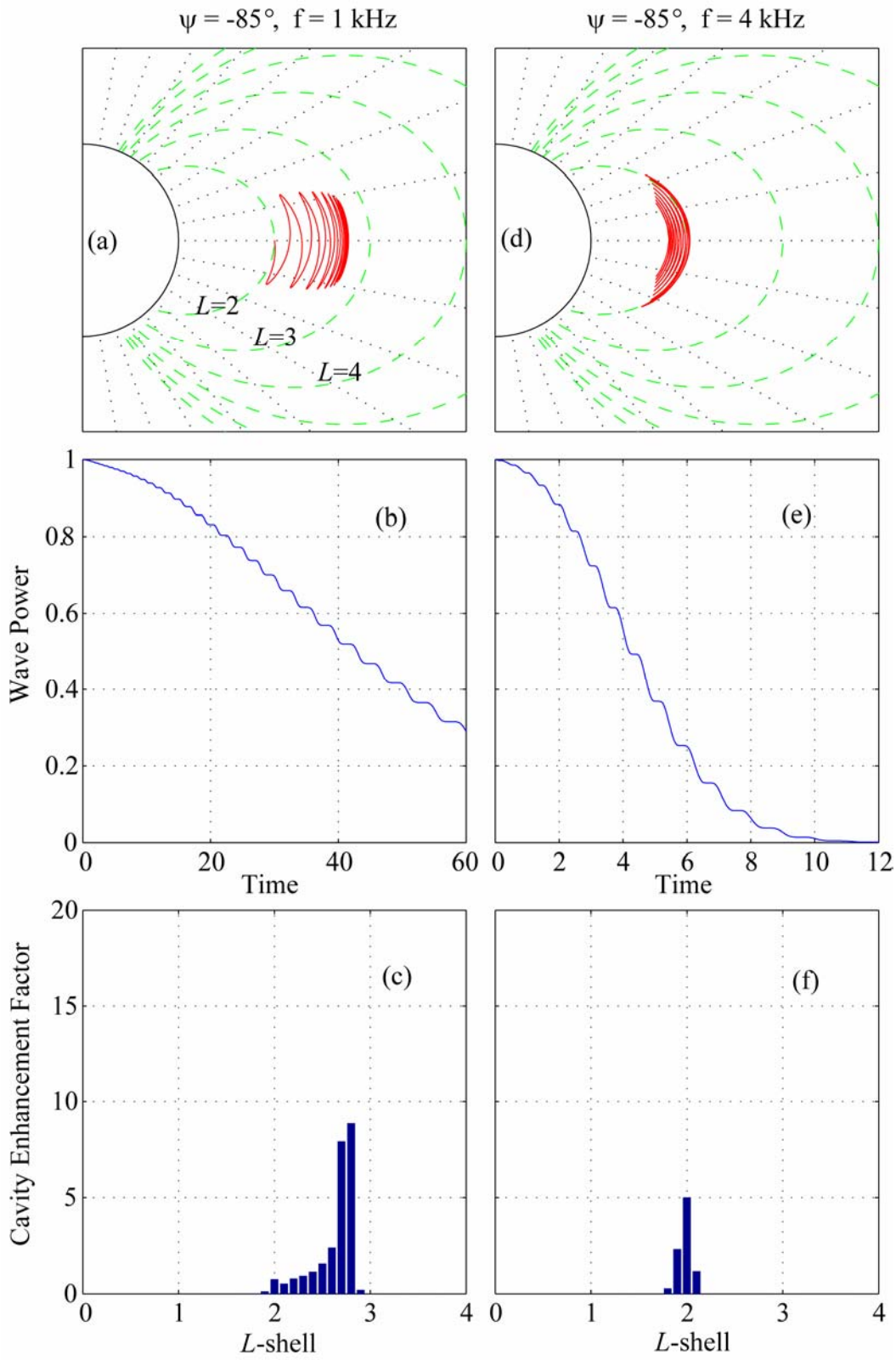

Figure 4: (a) - (f) Similar to before, but for 1-kHz and 4-kHz waves.

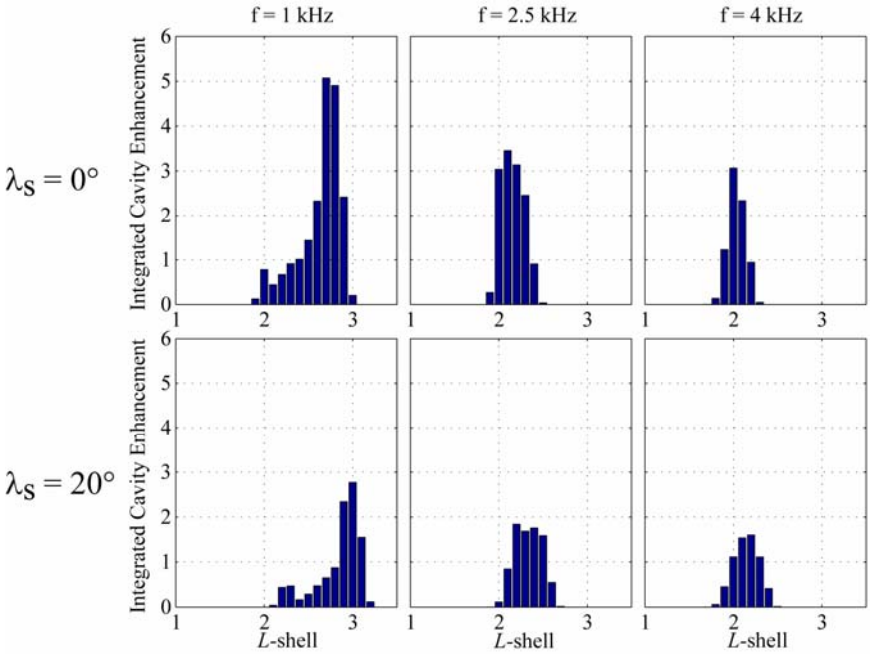

Figure 5: Cavity enhancement factor integrated over all wave normal angles considered. Result is normalized by the total number of injections. The cavity enhancement is shown at L-shells from $1 < L < 3.5$ for 1-kHz, 2.5-kHz and 4-kHz waves injected from $L = 2$; with equatorial injections shown across the top row and off-equatorial across the bottom row.

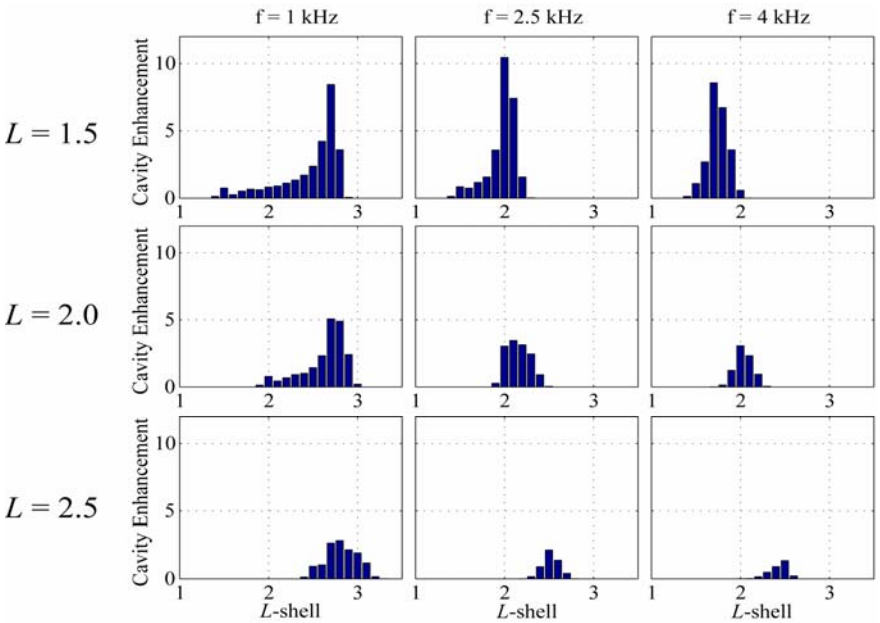

Figure 6: The three columns display the three sample wave frequencies of 1 kHz, 2.5 kHz, and 4 kHz; and each row represents the three separate injection source sites (L = 1.5, 2.0 and 2.5). All waves were injected from the magnetic equator.

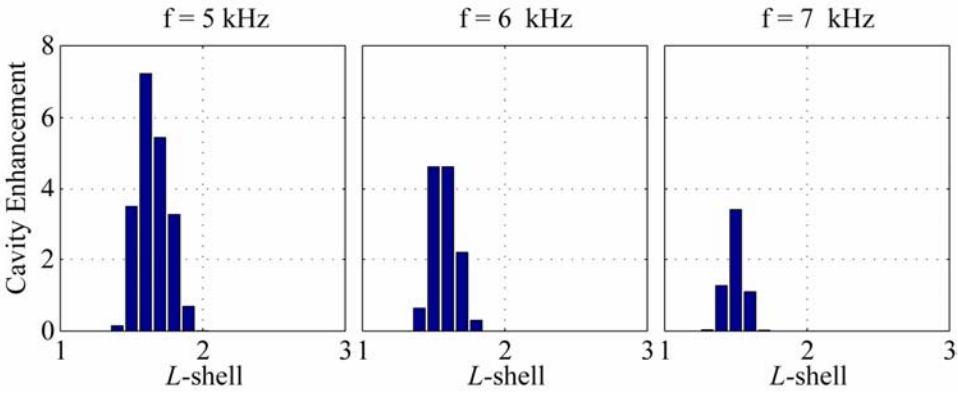

Figure 7: Integrated cavity enhancement factor for injection from the geomagnetic equator at $L = 1.5$, where the equatorial f_{LHR} is approximately 6 kHz.

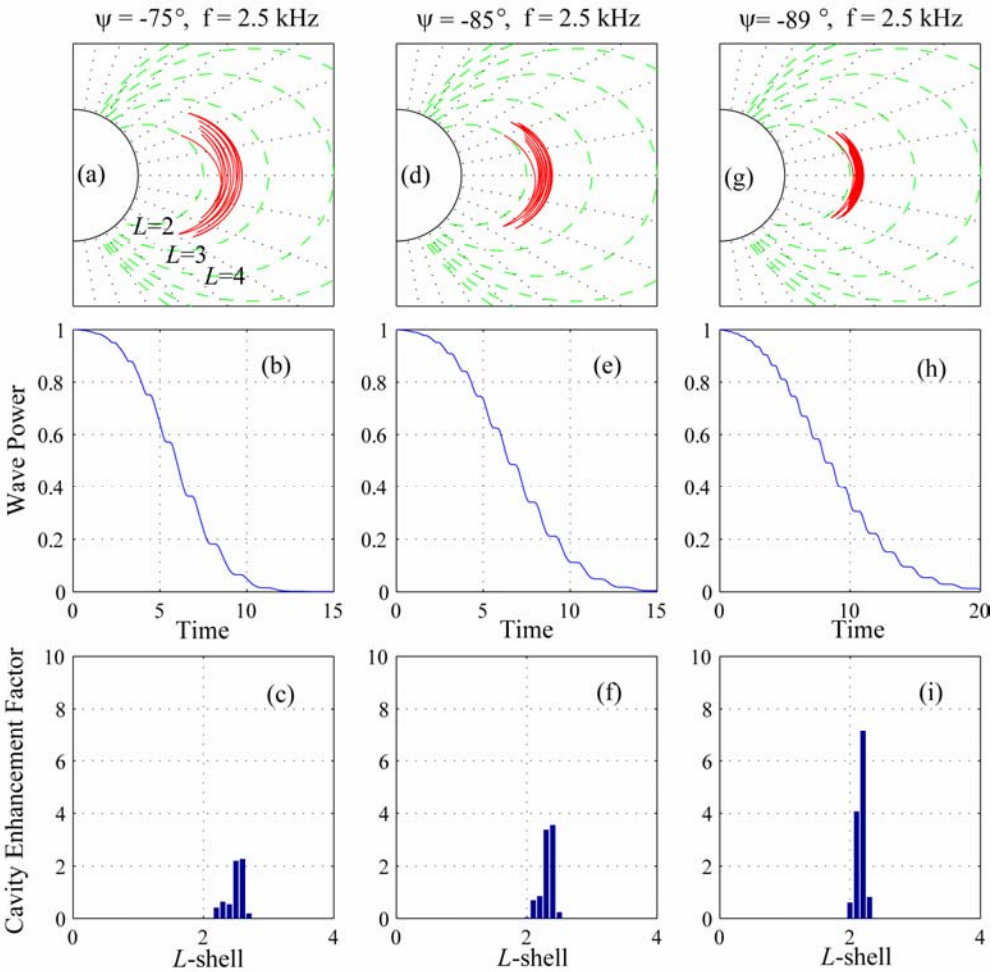

Figure 8: (a) – (i) Similar to before, with parameters indicated on plots. All rays were injected at $L = 2$ at $\lambda = 20^{o}$.

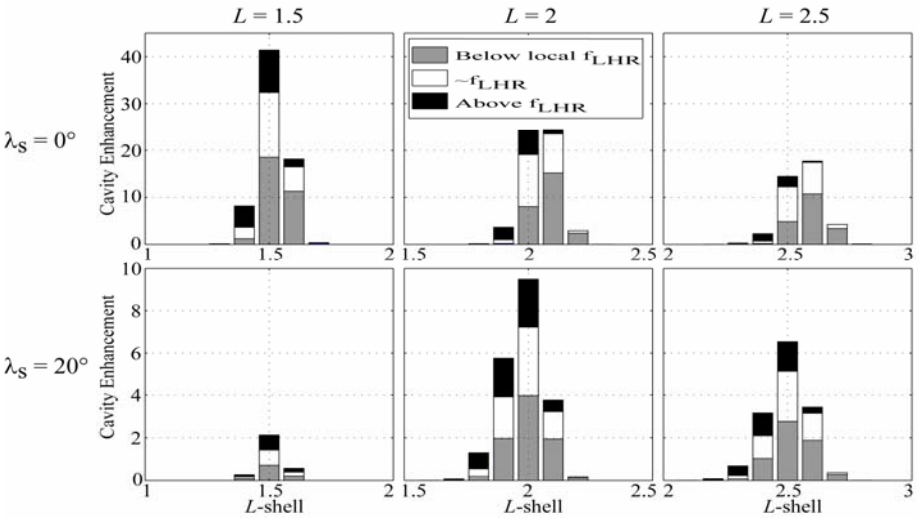

Figure 9: The effects of incorporating the frequency and angular limitations imposed by the use of short antennas in a magnetoplasma

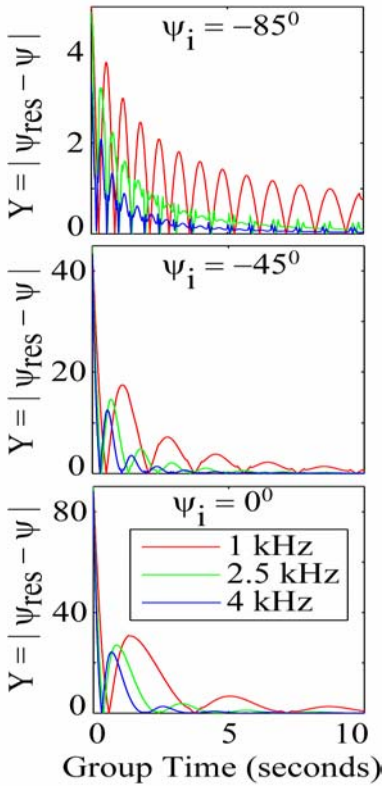

Figure 10: (a) - (c) $Y = | \psi - \psi_{res} |$ for three different wave frequencies and initial wave normal angles, all injected from the equator at $L = 2$. The quasi-periodicity seen is a result of repeated magnetospheric reflections along the ray path. Note that regardless of frequency or initial wave normal angle, ψ rapidly ends up very close to the resonance cone.

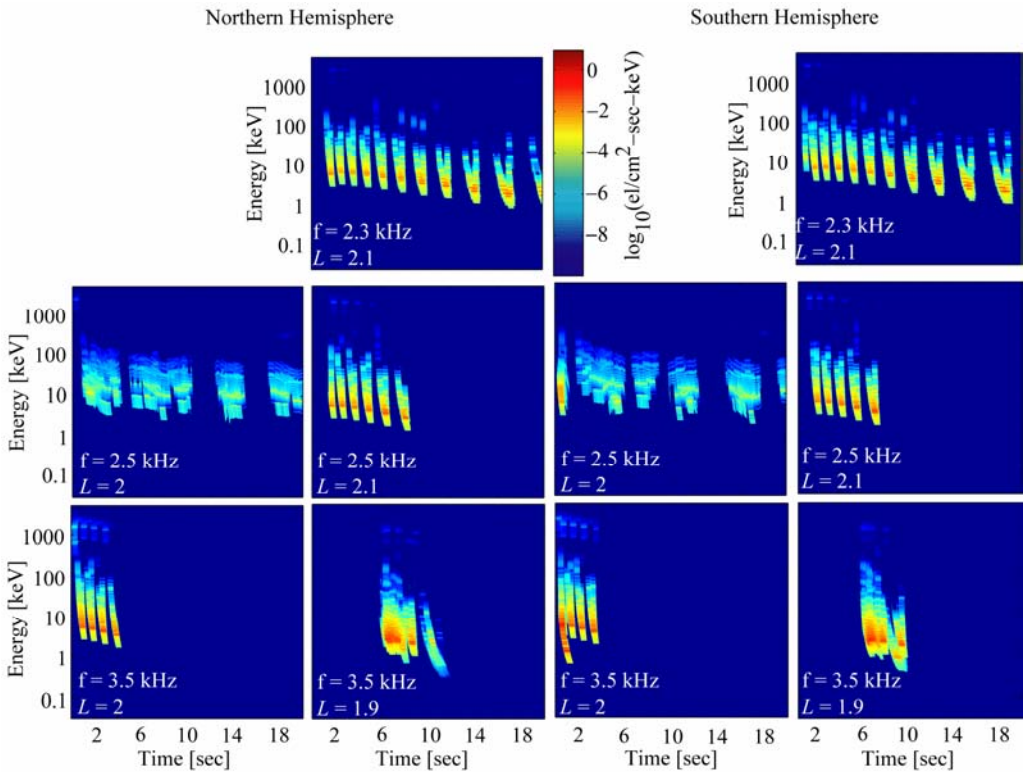

Figure 11: Differential number flux at 100-km altitude induced by an equatorial source at $L = 2$. The left (right) two columns display the flux induced at the northern (southern) hemisphere.

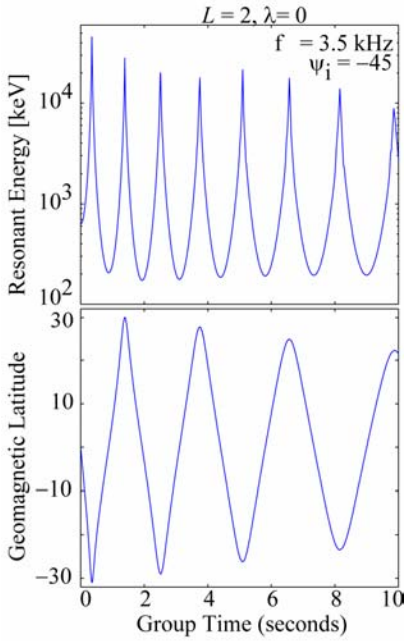

Figure 12: The top panel shows resonant electron energy along the ray path for the m = 1 resonance mode for a 3.5-kHz wave injected from the equator at $L = 2$. The bottom panel shows geomagnetic latitude along ray path. Note that E_{res} increases off the equator, and that the resonant energy stays above 100 keV at all points along the ray path.

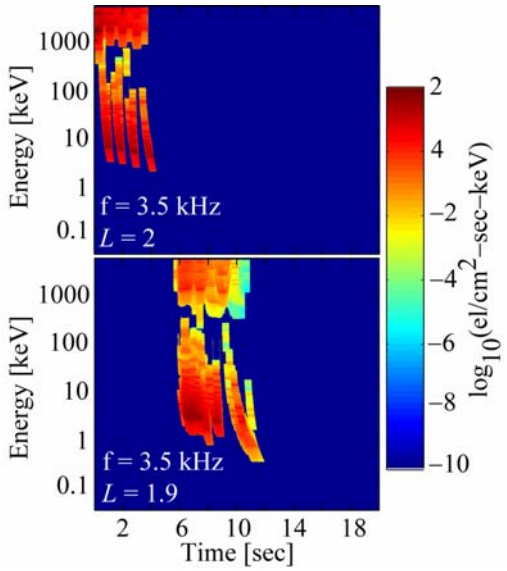

Figure 13: Differential number flux in the northern hemisphere at $L = 2$ and $L = 1.9$ induced by a 3.5-kHz equatorial source at $L = 2$. These results used a constant energetic electron distribution function of 50,000 cm^{-2}-s^{-1}-$ster^{-1}$-keV^{-1} with a square loss-cone.

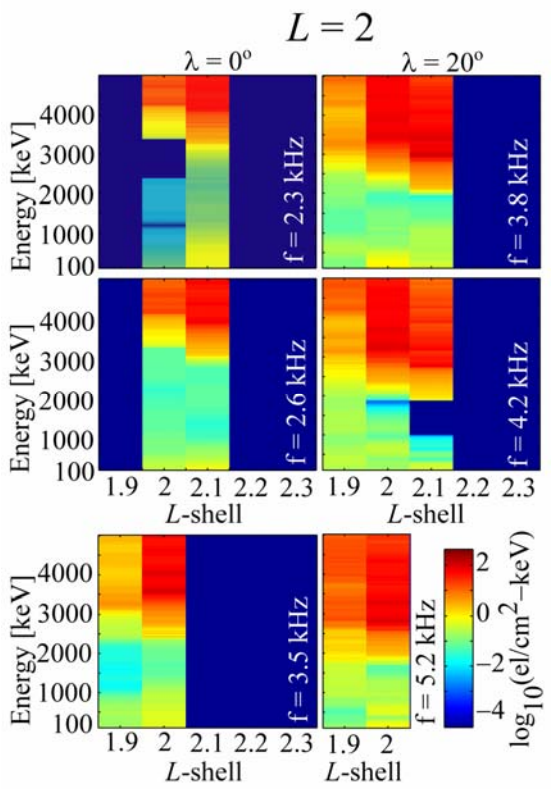

Figure 14: Precipitation and illumination spectra induced by sources at $L = 2$, at the geomagnetic equator and a latitude of 20^{o}. These results were obtained by integrating the differential number flux over time.

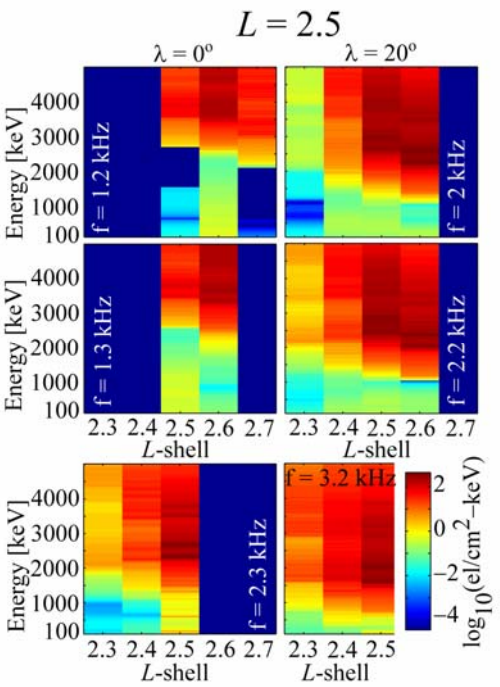

Figure 15: Similar to Figure 14, except for sources at $L = 2.5$. Although the region of illumination is at higher L-shells, the general trends are similar and explained in the text.

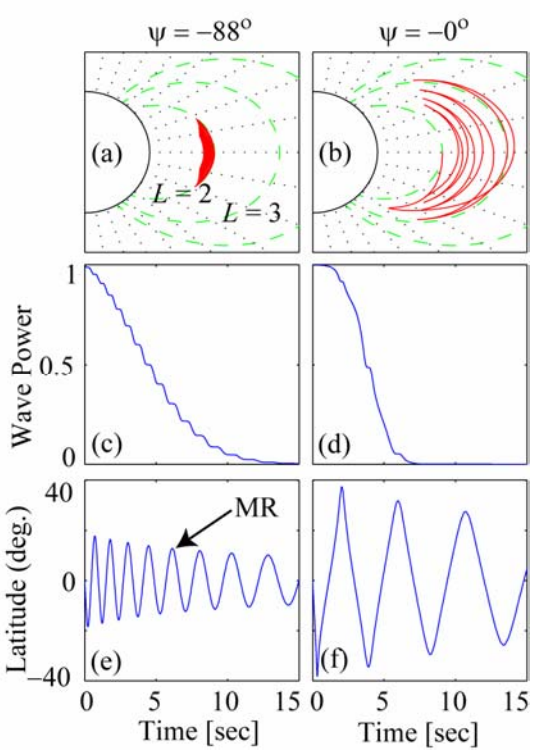

Figure 16: Ray paths, Landau damping and latitude along ray path for two 3.5-kHz rays injected from $L = 2$. The left column displays these parameters for a ray with an initial wave normal angle of -88°, while the right column is for $\psi = 0°$.

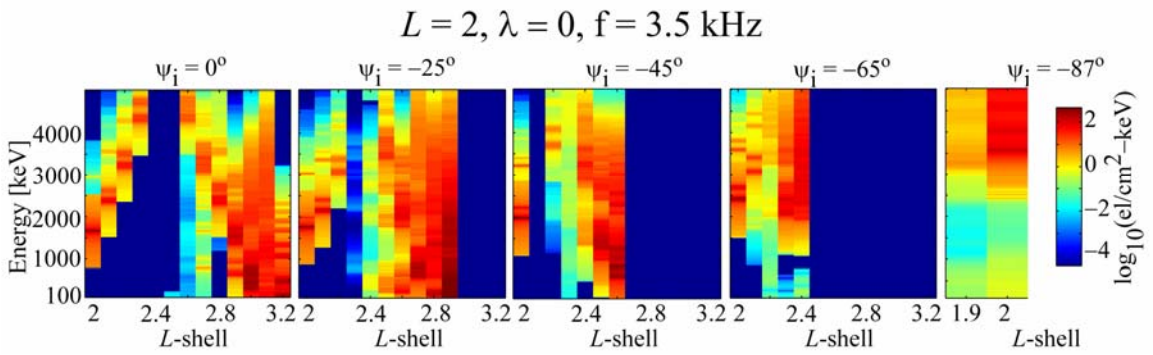

Figure 17: Precipitation spectra for 3.5-kHz waves injected at a range of initial wave normal angles. Note that lower initial ψ spreads wave power over a broader range of *L*-shells, but the precipitation signature is generally weaker at higher energies.

REFERENCES

Abel, B., and R. M. Thorne, Electron scattering loss in the Earth's inner magnetosphere: 1. Dominant physical processes, *J. Geophys. Res., 103*, 2385, 1998a. (Correction, *J. Geophys. Res., 104*, 4627, 1999.)

Abel, B., and R. M. Thorne, Electron scattering loss in the Earth's inner magnetosphere: 2. Sensitivity to model parameters, *J. Geophys. Res., 103*, 2397, 1998b. (Correction, *J. Geophys. Res., 104*, 4627, 1999.)

Albert, J. M., Analysis of quasi-linear diffusion coefficients, *J. Geophys. Res., 104*, 2429, 1999.

Angerami, J. J., and J. O. Thomas, Studies of planetary Atmospheres, 1, The distribution of electrons and ions in the Earth's exosphere, *J. Geophys. Res., 69*, 4537, 1964.

Baker, D. N., The occurrence of operational anomalies in spacecraft and their relationship to Space Weather, *IEEE Trans. Plasma Sci., 28*, 2007, 2000.

Bell, T.F., The Nonlinear Gyroresonance Interaction between Energetic Electrons and Coherent VLF Waves Propagating at an Arbitrary Angle with Respect to the Earths Magnetic-Field, *J. Geophys. Res., 89* (A2), 905-918, 1984.

Bell, T. F., U. S. Inan, J. Bortnik, and J. D. Scudder, The Landau damping of magnetospherically reflected whistlers within the plasmasphere, *Geophys. Res. Lett.*, 29(15), 1733, doi:10.1029/2002GL014752, 2002.

Bortnik J., U. S. Inan, and T. F. Bell, Temporal signatures of radiation belt electron precipitation induced by lightning generated MR whistler waves. Part I: Methodology, *J. Geophys. Res., 111*, A02204, doi:10.1029/2005JA011182, 2006a.

Bortnik J., U. S. Inan, and T. F. Bell, Temporal signatures of radiation belt electron precipitation induced by lightning generated MR whistler waves. Part II: Global signatures, *J. Geophys. Res., 111*, A02205, doi:10.1029/2005JA011398, 2006b.

Budden, K. G., *The Propagation of Radio Waves*, Cambridge Univ. Press, New York, 1985.

Cair'o, L., and F. Lefeuvre, Localization of sources of ELF/VLF hiss observed in the magnetosphere: Three-dimensional ray traycing, *J. Geophys. Res., 91*, 4352, 1986.

Carpenter, D.L., and R.R. Anderson, An ISEE/Whistler model of equatorial electron-density in the magnetosphere. *J. Geophys. Res., 97* (A2), 1097-1108, 1992.

Edgar, B. C., The structure of the magnetosphere as deduced from magnetospherically reflected whistlers, *Tech. Rep. 3438-2*, Radiosc. Lab., Stanford Electron. Lab., Stanford Univ., Stanford, Cali., 1972.

Edgar, B. C., The upper and lower frequency cutoffs of magnetospherically reflected whistlers, *J. Geophy. Res., 81*, 205, 1976.

Hashimoto, K., I. Kimura and H. Kumagai, Estimation of electron temperature by VLF waves propagating in directions near the resonance cone, *Planet. Space Sci., 25*, 871, 1977.

Inan, U. S., and T. F. Bell, The plasmapause as a VLF waveguide, J. Geophys. Res., 82, 2819, 1977.

Inan, U.S., T.F. Bell, and H.C. Chang, Particle-Precipitation Induced by Short-Duration VLF Waves in the Magnetosphere, *J. Geophys. Res., 87* (A8), 6243-6264, 1982.

Inan, U. S., Gyroresonant pitch angle scattering by coherent and incoherent whistler mode waves in the magnetosphere, *J. Geophys. Res., 92*, 127, 1987.

Inan, U. S., and T. F. Bell, Pitch angle scattering of energetic particles by oblique whistler waves, *Geophys. Res. Lett., 18*, (1), 49-52, 1991.

Inan, U. S., T. F. Bell, J. Bortnik, and J. M. Albert, Controlled precipitation of radiation belt electrons, *J. Geophys. Res., 108* (A5), 1186, doi:10.1029/2002JA009580, 2003.

Jasna, D., U. S. Inan, and T. F. Bell, Equatorial gyroresonance between electrons and magnetospherically reflected whistlers, *Geophys. Res. Lett., 17*, (11), 1865-1868, 1990.

Kennel, C. F., and H. E. Petschek, Limit on stably trapped particle fluxes, *J. Geophys. Res., 99* (1), 1966.

Kulkarni, P., U. S. Inan, and T. F. Bell (2006), Whistler mode illumination of the plasmaspheric resonant cavity via in situ injection of ELF/VLF waves, *J. Geophys. Res., 111*, A10215, doi:10.1029/2006JA011654.

Lyons, L. R., R. M. Thorne, and C. F. Kennel, Pitch angle diffusion of radiation belt electrons within the plasmasphere, *J. Geophys. Res., 77*, 3455, 1972.

Vette, J., The AE-8 trapped electron model environment, *National Space Science Data Center*, Report 91-24, Greenbelt, Maryland, 1991.

Walt, M., *Introduction to geomagnetically trapped radiation*, Cambridge University Press, 1994.